Plant Physiology Preview. Published on April 21, 2020, as DOI:10.1104/pp.20.00284

Short title: CytM decreases photosynthesis under photomixotrophy

Corresponding author: Yagut Allahverdiyeva, allahve@utu.fi

Cytochrome c_M decreases photosynthesis under photomixotrophy in *Synechocystis* sp. PCC 6803

Daniel Solymosi, Lauri Nikkanen, Dorota Muth-Pawlak, Duncan Fitzpatrick, Ravendran Vasudevan, Christopher J. Howe, David J. Lea-Smith, Yagut Allahverdiyeva*

Laboratory of Molecular Plant Biology, Department of Biochemistry, University of Turku, Turku FI–20014, Finland (D.S., L.N., D.M.P., D. F., Y.A.)
Department of Biochemistry, University of Cambridge, Cambridge CB2 1QW, United Kingdom (R.V., C.J.H., D.J.L-S.)
School of Biological Sciences, University of East Anglia, Norwich NR4 7TJ, United Kingdom (D.J.L-S.)
*Corresponding author

One-sentence summary: A cryptic, highly conserved cytochrome accelerates inhibition of photosynthesis in *Synechocystis* under long-term photomixotrophy.

Author contributions: D.S. and Y.A. designed the research. D.S. performed the majority of the experiments. D.M.P. and D.S. performed and analysed proteomics data. L.N. performed Cyt*f* kinetic measurements and immunoblotting. D.J.L-S. constructed the mutant strains. All authors contributed to analysing the data. D.S., Y.A., and D.J.L-S wrote the paper. All authors revised the manuscript.

Abstract

Photomixotrophy is a metabolic state which enables photosynthetic microorganisms to simultaneously perform photosynthesis and metabolism of imported organic carbon substrates. This process is complicated in cyanobacteria, since many, including Synechocystis (*Synechocystis* sp. PCC 6803), conduct photosynthesis and respiration in an interlinked thylakoid membrane electron transport chain. Under photomixotrophy, the cell must therefore tightly regulate electron fluxes from photosynthetic and respiratory complexes. In this study, we demonstrate, via characterization of photosynthetic apparatus and the proteome, that photomixotrophic growth results in a gradual inhibition of Q_A^- re-oxidation in wild-type Synechocystis, which largely decreases photosynthesis over three days of growth. This process is circumvented by deleting the gene encoding cytochrome c_M (CytM), a cryptic *c*-type heme protein widespread in cyanobacteria. The ΔCytM strain maintained active photosynthesis over the three-day period, demonstrated by high photosynthetic O_2 and CO_2 fluxes and effective yields of photosystems I and II. Overall, this resulted in a higher growth rate than wild type, which was maintained by accumulation of proteins involved in phosphate and metal uptake, and cofactor biosynthetic enzymes. While the exact role of CytM has not been determined, a mutant deficient in the thylakoid-localised respiratory terminal oxidases and CytM (ΔCox/Cyd/CytM) displayed a similar phenotype under photomixotrophy to ΔCytM. This, in combination with other physiological data, suggests that CytM does not transfer electrons to these complexes, which had previously been hypothesized. In summary, our data suggest that CytM may have a regulatory role in photomixotrophy by modulating the photosynthetic capacity of cells.

Introduction

Switching between different trophic modes is an advantageous feature, which provides great metabolic flexibility for cyanobacteria. For a long time, these photosynthetic prokaryotes were considered as a group of predominantly photoautotrophic organisms (Smith 1983, Stal and Moezelaar 1997). Lately, accumulating evidence marks the physiological and ecological importance of trophic modes involving organic carbon assimilation, *e.g.* photomixotrophy (Zubkov and Tarran 2008, Moore et al 2013). Dissolved organic carbon, most notably monosaccharides, including glucose and fructose, accumulates in the environment, mainly during phytoplankton blooms (Teeling et al 2012, Ittekot et al 1981). During photomixotrophy, photosynthetic organisms must balance the consumption of organic carbon sources with photosynthesis and carbon fixation.

In the model cyanobacterium Synechocystis (*Synechocystis* sp. PCC 6803), photomixotrophy is further complicated by the operation of anabolic and catabolic processes occurring in the same cellular compartment and by the presence of an interlinked thylakoid membrane-localised electron transport pathway involved in both photosynthesis and respiration (Vermaas et al., 2001; Mullineaux, 2014; Lea-Smith et al., 2016). In Synechocystis, photosynthetic linear electron flow is similar to other oxygenic photoautotrophs. In photosystem (PS) II and PSI, the energy of the harvested photons induces charge separation. Electrons from the PSII primary donor P680 pass via pheophytin and the primary quinone Q_A, to the secondary quinone, Q_B. Oxidized $P680^+$ is the strongest biological oxidizing molecule, which drives water splitting on the luminal side of PSII. When Q_B is doubly reduced, it binds two protons from the cytosol, converting plastoquinone (PQ) to plastoquinol (PQH_2), which then diffuses into the membrane PQ pool. Cytochrome (Cyt) b_6f receives two electrons from PQH_2 and transfers an electron to the mobile small protein, plastocyanin (Pc) or cytochrome c_6 (Cyt c_6). An electron is subsequently transferred to PSI, replacing a newly excited electron that is transferred from the PSI reaction center $P700^+$ via several co-factors to ferredoxin (Fed). Lastly, electrons are transferred from Fed to $NADP^+$ by ferredoxin-$NADP^+$ reductase (FNR) to generate NADPH. In the respiratory electron transfer pathway, PQ is reduced by NAD(P)H dehydrogenase-like complex I (NDH-1) and succinate dehydrogenase (SDH), using electrons ultimately derived from Fed (Schuller et al., 2019) and succinate, respectively. Electrons from the PQ-pool can be transferred to a thylakoid-localized respiratory terminal oxidase (RTO), cytochrome *bd*-quinol oxidase (Cyd), or via Cyt b_6f and Pc/Cyt c_6 to a second RTO, an aa_3-type cytochrome-*c* oxidase complex (Cox). How Synechocystis regulates electron input from PSII and the NDH-1 and SDH complexes into the photosynthetic electron transport chain and to RTOs under photomixotrophic conditions is not fully understood. Moreover, Synechocystis encodes four isoforms of the flavodiiron proteins (FDPs), Flv1-4, which likely utilize NAD(P)H (Vicente et al., 2002; Brown et al., 2019) or reduced Fed (Santana-Sanchez et al., 2019). These proteins function in light-induced O_2 reduction as hetero-oligomers consisting of Flv1/Flv3 and/or Flv2/Flv4 (Helman et al., 2003; Mustila et al., 2016; Allahverdiyeva et al., 2015; Santana-Sanchez et al., 2019).

In Synechocystis, the water-soluble Cyt c_6 (formerly referred to as Cyt c_{553}) can substitute for Pc under conditions of copper deprivation (Durán et al., 2004). Cyt c_6 belongs to the Cyt *c* family, whose members are characterized by a covalently bound *c*-type heme cofactor. *C*-type Cyts are further classified into groups such as the Cyt c_6-like proteins, Cyt c_{555}, Cyt c_{550}, and CytM (Bialek et al., 2008). Apart from the well-established role of Cyt c_6 in electron transfer (Kerfeld and Krogman, 1998) and the role of Cyt c_{550} (PsbV) in stabilizing the PS II water splitting complex (Shen and Inoue, 1993), most of the Cyt *c* proteins remain enigmatic.

Cyt c_M (CytM) is conserved in nearly every sequenced cyanobacterium with the exception of the obligate symbionts *Candidatus acetocyanobacterium thalassa* and *Candidatus Synechococcus spongiarum* (Supplemental Fig. S1; Bialek et al., 2016). In Synechocystis, CytM is encoded by *sll1245* (Malakhov et al., 1994). Nevertheless, its subcellular location is ambiguous. An early study localised CytM to the thylakoid and plasma membranes in 'purified' membrane fractions (Bernroitner et al., 2009). However, cross contamination between membranes was not determined, which has been an issue in studies using similar separation techniques (Sonoda et al., 1997; Schultze et al., 2009). In later proteomics studies, CytM has not been detected or localised using membranes purified by either two-phase aqueous polymer partitioning or subcellular fractionation (Baers et al., 2019). However, the structure of the hydrophobic N-terminus resembles a signal peptide, which suggests that CytM is targeted to a membrane. Sequence similarity to the N-terminus cleavage site of Synechocystis Cyt c_6 suggests that the N-terminus is processed and the mature 8.3 kDa protein is inserted into the lumen (Malakhov et al., 1994). However, cleavage does not seem to occur *in vivo,* as the protein extracted from various cyanobacterial species, including Synechocystis*, Synechococcus elongatus* PCC 6301, and *Anabaena* sp. PCC 7120, was found to be around 12 kDa (Cho et al., 2000; Bernroitner et al., 2009), implying that the hydrophobic N-terminus remains on the protein and serves as a membrane anchor. The subcellular location of CytM and whether it is membrane anchored is therefore still unknown.

It has been suggested that CytM may play a role in respiratory or photosynthetic electron transfer (Manna and Vermaas, 1997; Bernroitner et al., 2009). In Synechocystis, CytM was shown to reduce the Cu_A center of Cox *in vitro* with similar efficiency as Cyt c_6 (Bernroitner et al., 2009). However, given the midpoint potential of CytM (+150 mV), electron transfer from Cyt*f* (+320 mV) to CytM would be energetically uphill (Cho et al 2000). Notably*,* CytM is unable to reduce PSI *in vitro* (Molina-Heredia et al., 2002). Thus, it is difficult to see how the protein would substitute for Cyt c_6 or Pc. Importantly, CytM is not detected under photoautotrophic conditions (Baers et al., 2019) and deletion of the gene does not affect net photosynthesis or dark respiratory rates (Malakhov et al., 1994) under these conditions. Cold, high light, and salt stress, however, induce gene expression and the stress-induced co-transcriptional regulation between *cytM* (CytM), *petJ* (Cyt c_6), and *petE* (Pc) suggests a stress-related role in electron transfer (Malakhov et al., 1999).

Besides environmental stresses, CytM has been linked to organic carbon-assimilating trophic modes. A dark-adapted variant of *Leptolyngbya boryana* was found to grow faster than wild type (WT) in heterotrophy. Genome re-sequencing revealed that the fast-growing strain harboured a disrupted *cytM* (Hiraide et al., 2015). In line with this, the *cytM* deletion mutant of Synechocystis demonstrated a growth advantage over the WT under dark and light-activated heterotrophic conditions, and under photomixotrophic conditions (Hiraide et al., 2015). Under dark heterotrophic conditions, ΔCytM had higher dark respiration and net photosynthesis. However, the physiological mechanism and the functional role of CytM remains entirely unknown.

In this study, we sought to uncover the bioenergetics of photomixotrophically grown Synechocystis and physiological background behind the growth advantage of ΔCytM by characterizing its photosynthetic machinery and the proteomic landscape. We demonstrate gradual inhibition of Q_A^- re-oxidation, resulting in repression of linear electron transport and CO_2 fixation in Synechocystis during photomixotrophic growth. A mutant lacking CytM circumvents inhibition of Q_A^- re-oxidation during photomixotrophic growth, enabling higher rates of net photosynthesis. In order to meet the substrate demand for enhanced growth, the mutant retains transporter proteins, cofactor biosynthetic enzymes, and slightly adjusts central carbon metabolism compared to photomixotrophic WT. Although the function of CytM was previously associated with Cox, both thylakoid respiratory terminal oxidases, Cox and Cyd, were found to be dispensable for the metabolic advantage conferred by deletion of CytM in photomixotrophy. We conclude that when cells are exposed to high glucose conditions, CytM reduces the photosynthetic capacity and contributes to regulating the redox state of the intertwined photosynthetic and respiratory electron transport chain, in order to accommodate this new energy source.

Results

Deletion of CytM confers a growth advantage on ΔCytM and ΔCox/Cyd/CytM in photomixotrophy

In order to elucidate the physiological role of CytM and its possible functional association with thylakoid-localised RTOs, we studied the ΔCytM, ΔCox/Cyd, and ΔCox/Cyd/CytM mutants. Unmarked mutants of Synechocystis lacking CytM were constructed by disrupting the *cytM* gene (*sll1245*) in WT (Supplemental Fig. S2) and the ΔCox/Cyd mutant (Lea-smith et al., 2013). Strains were then pre-cultured under photoautotrophic conditions at 3% CO_2 and examined under a range of different growth conditions at air level CO_2.

First, we determined whether deletion of *cytM* affected photoautotrophic growth by culturing cells under moderate constant 50 μmol photons m^{-2} s^{-1} light. In line with previous studies (Malakhov et al., 1994; Hiraide et al., 2015), no growth difference was observed between ΔCytM and WT under photoautotrophic conditions (Fig. 1A).

Next, we characterized growth under photomixotrophic conditions. To determine how different starting glucose concentrations affected photomixotrophic growth (Fig. 1A, B), we supplemented the medium with 5 mM and 10 mM glucose and cultivated the strains under constant 50 μmol photons m^{-2} s^{-1} light. Based on optical density measurements (OD_{750}), all cultures with added glucose grew substantially faster than those cultured photoautotrophically (Fig. 1A, B). Deletion of *cytM* had no effect on cells grown at 5 mM glucose. However, when cultured with 10 mM glucose, ΔCytM demonstrated 1.9±0.4 (P=6E-6) higher OD_{750} than WT and ΔCox/Cyd/CytM demonstrated 1.9±0.6 (P=0.002) higher OD_{750} compared to ΔCox/Cyd, after three days. In line with this, ΔCytM consumed more glucose than WT (Fig. 2A), as quantified by measuring the glucose concentration of the cell-free spent media on the third day of photomixotrophic growth.

We next characterized growth under photomixotrophic conditions but with different light regimes (Fig. 1C, D), either constant 10 μmol photons m^{-2} s^{-1} light (low light photomixotrophy) or 15 min 50 μmol photons m^{-2} s^{-1} light every 24 h (LAHG, light-activated heterotrophic growth). These cultures were supplemented with 10 mM starting glucose. Interestingly, under low light photomixotrophy, neither ΔCytM nor ΔCox/Cyd/CytM demonstrated a growth advantage compared to WT and ΔCox/Cyd, respectively. Under LAHG condition, ΔCytM grew faster than WT as previously reported (Hiraide et al., 2015). The ΔCox/Cyd and ΔCox/Cyd/CytM mutants were unable to grow under LAHG. Previously, it was reported that Cox is indispensable under this condition (Pils et al., 1997).

We next examined the morphology of ΔCytM and WT cells on the third day of photomixotrophic growth (10 mM glucose, 50 μmol photons m^{-2} s^{-1} constant light), when the highest difference in OD_{750} was observed. Cell size, cell number per OD_{750}, and chlorophyll (chl) concentration per cell were determined. No difference was observed in cell size between ΔCytM and WT (Supplemental Fig. S3), and the cell number per OD_{750} was similar in both strains (Fig. 2B), confirming that the difference in OD_{750} reflects higher growth.

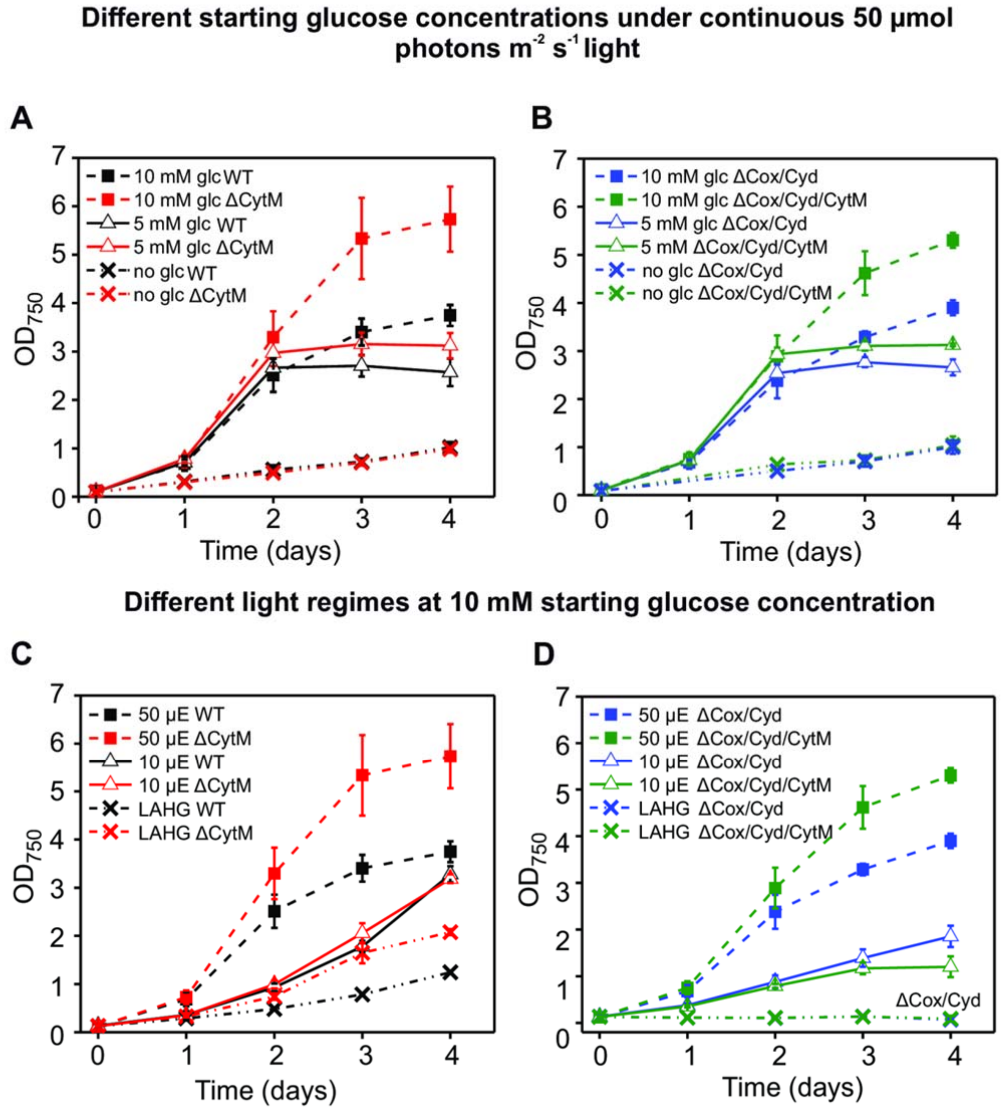

Figure 1. Impact of different glucose concentrations and light regimes on the growth of wild type (WT), ΔCytM, ΔCox/Cyd, and ΔCox/Cyd/CytM. Cultures were exposed to 50 µmol photons m^{-2} s^{-1} light (A, B) and were grown under photoautotrophic conditions without glucose (dash-dot-dot line) or under photomixotrophic conditions with 5 mM glucose (solid line) or 10 mM glucose (dashed line). Growth was then assessed under various light regimes in cultures containing 10 mM glucose (C, D), under constant 50 µmol photons m^{-2} s^{-1} light (dashed line), constant 10 µmol photons m^{-2} s^{-1} light (solid line) and light-activated heterotrophic growth (LAHG) a light regime of 15 min of 50 µmol photons m^{-2} s^{-1} light exposure every 24 h (dash-dot-dot line). Values are means ± SD, n = 3-7 biological replicates.

However, the chl *a* content per cell increased in ΔCytM (Fig. 2C), suggesting that the photosystem content or PSII/PSI ratio has been altered in this strain.

Overall, the most pronounced growth advantage of ΔCytM over WT was observed when cells were exposed to a light intensity of 50 µmol photons m^{-2} s^{-1} and glucose concentration of 10 mM. Therefore, these conditions were used for all subsequent phenotyping experiments examining cells cultured photomixotrophically. The same phenotype manifested in the triple ΔCox/Cyd/CytM mutant, showing that Cox and Cyd are not required for the growth advantage. Moreover, we demonstrate that deletion of *cytM* leads to a higher cellular

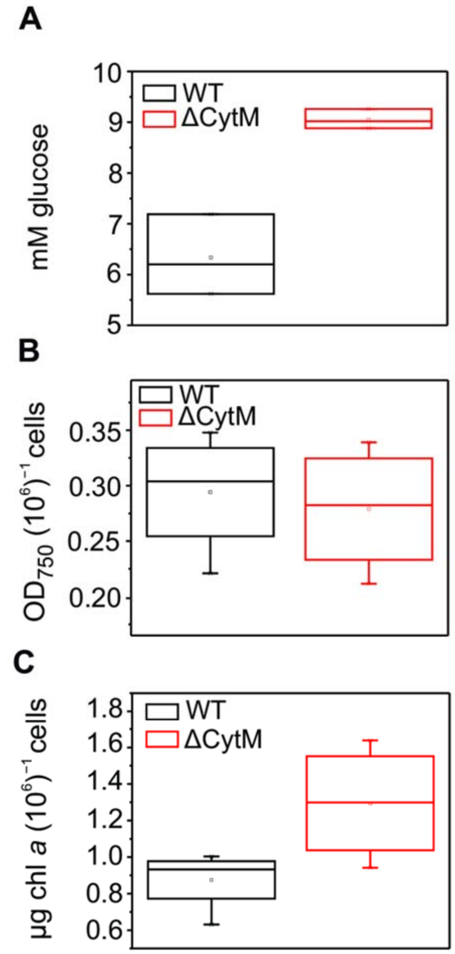

Figure 2. Glucose consumption, cellular chl content, and cell number of WT and ΔCytM cultures on the third day of photomixotrophic growth. Amount of glucose consumed by the cells (A) was deduced from the remaining glucose in spent media on the third day. This number reflects the consumption of the whole culture rather than the glucose uptake rate of a given number of cells. Optical density per cell number (B) and cellular chl content (C) were determined. Values are means ± SD, n = three biological replicates. Cultures were grown photomixotrophically under constant 50 µmol photons m^{-2} s^{-1} illumination supplemented with 10 mM glucose. Samples were taken on the third day.

chl *a* content, which implies an altered photosynthetic machinery when cells are cultured photomixotrophically.

Deletion of CytM circumvents inhibition of Q_A^- re-oxidation under photomixotrophy

To determine how long-term exposure to photomixotrophy affects the photosynthetic machinery of Synechocystis WT and how deletion of CytM rescues this phenotype, we first analyzed net photosynthesis by probing the O_2 evolution capacity of cells (Fig. 3E). When WT cells were grown photomixotrophically, only marginal net photosynthetic O_2 evolution was observed on the third day. Strikingly, in the presence of the artificial electron acceptor, 2,6-dichloro-*p*-benzoquinone (DCBQ), the O_2 evolving capacity of photomixotrophically

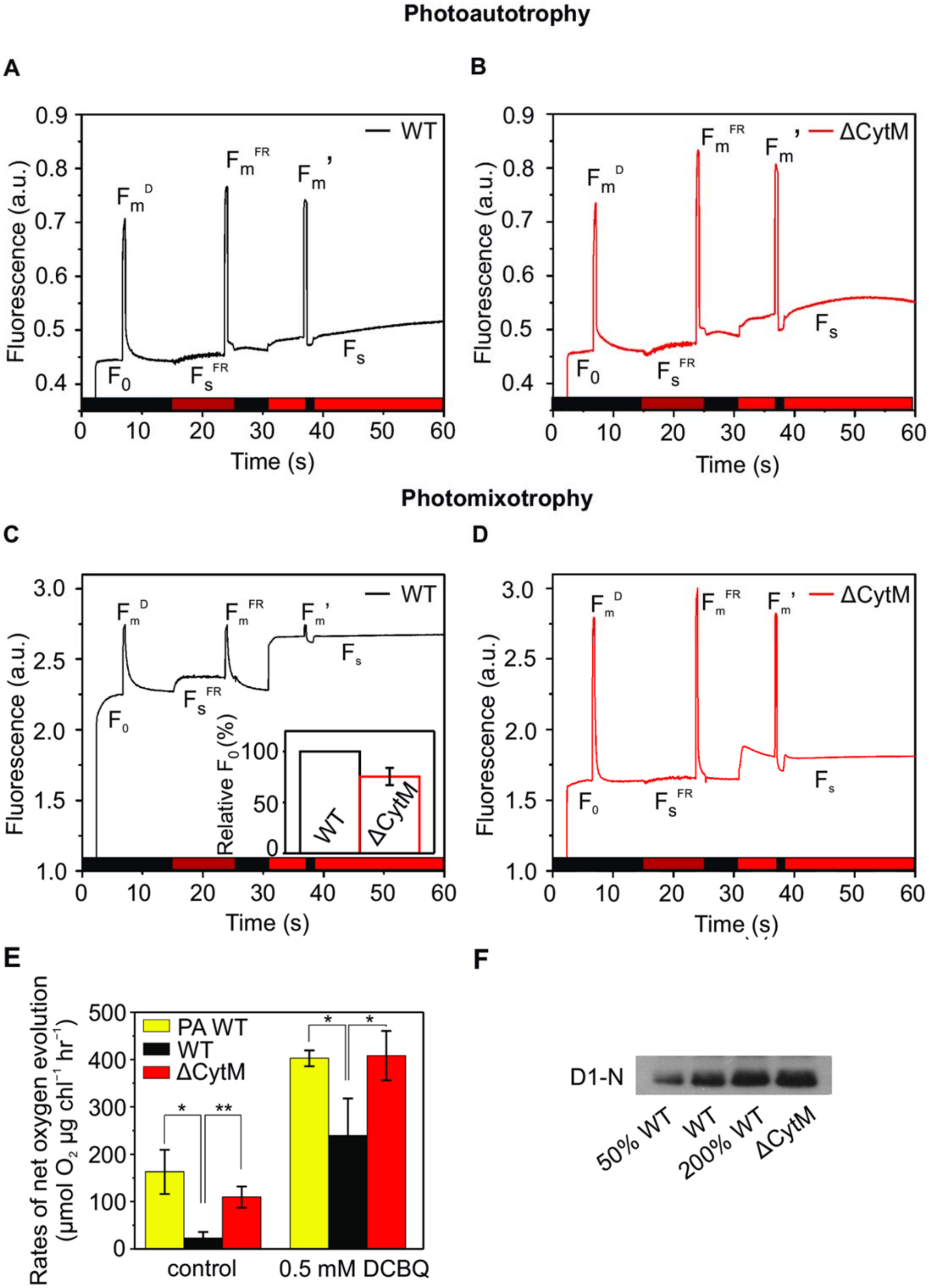

grown WT increased, although not to the level of the photoautotrophically cultured WT. DCBQ accepts electrons from Q_A and/or Q_B, disconnecting PSII from the downstream electron transfer chain (Srivastava et al., 1995). This suggests that a high proportion of PSII complexes are functional in photomixotrophically cultured WT and that inhibition of net photosynthesis is induced by a blockage downstream of PSII. Photomixotrophically grown ΔCytM demonstrated net photosynthetic O_2 production and PSII activity similar to photoautotrophically cultured WT, implying that deletion of CytM preserves photosynthetic activity under photomixotrophy. Immunoblotting performed on total protein extracts from photomixotrophically grown WT and ΔCytM demonstrated a higher accumulation of PSII reaction center protein D1 in ΔCytM compared to WT (Fig. 3F), suggesting that PSII levels are maintained in the mutant throughout photomixotrophic growth. The increased amount of D1 in ΔCytM likely contributes to the higher O_2 production compared to WT, although entirely accounting for the difference is unlikely.

Next, we assessed photosynthetic activity by probing chl fluorescence in WT and ΔCytM whole cells with multiple-turnover saturating pulses in dark, under far-red and under actinic red light (Fig. 3A-D). Compared to cells cultured photoautotrophically (Supplemental Fig. S4A), photomixotrophically grown WT cells demonstrated substantially higher initial fluorescence (F_0) and slower relaxation of pulse-induced fluorescence in the dark (see F_m^D relaxation in Fig. 3C), which suggests that the PQ pool is highly reduced. To verify this, cells were exposed to far-red light, which preferentially excites PSI, resulting in oxidation of the PQ-pool. If the PQ pool is highly reduced, then a lower steady-state fluorescence level (F_s) upon illumination of the cells with far-red light would be expected, similar to what was observed in the ΔCox/Cyd mutant (Ermakova et al. 2016). Interestingly, the opposite effect, a considerable increase in steady-state fluorescence, F_s^{FR}, was observed (Fig. 3C). This increase suggests inhibition of electron transport occurs at Q_B, since the negligible actinic effect of far-red is sufficient to reduce Q_A, resulting in increased fluorescence. Indeed, a similar rise in fluorescence was observed in photoautotrophically cultured WT when cells were measured in the presence of 3-(3,4-Dichlorophenyl)-1,1-dimethylurea (DCMU) (Supplemental Fig. S4C), a chemical, which occupies the Q_B site, thus blocking Q_A-to-Q_B forward electron transfer in PSII.

Moreover, the F_s level under steady-state actinic light was considerably higher compared to cells grown photoautotrophically and firing saturating pulses barely increased fluorescence (see F_m' on Fig. 3C), implying a highly reduced Q_A and negligible effective PSII yield (Y(II)) (Supplemental Fig. S5A). Similar results were observed in a different WT Synechocystis substrain commonly used in our laboratory (Supplemental Fig. S6) and in cells exposed to longer periods of illumination (Supplemental Fig. S7A). Taken together, these results suggest limited capacity to oxidize the PSII acceptor site, *i.e.* Q_A, in photomixotrophically cultured WT cells under illumination.

Compared to photomixotrophically grown WT, ΔCytM cultured under the same conditions demonstrated 24.8±8.3% lower F_0 and the pulse-induced fluorescence relaxation in darkness was markedly faster (see F_m^D on Fig. 3D). Far-red illumination did not increase fluorescence while saturating pulses greatly increased it (see F_m' on Fig. 3D), suggesting that the PSII effective yield Y(II) remained significantly higher, unlike in photomixotrophically grown WT cells (Supplemental Fig. S5A). Thus, in sharp contrast to WT, ΔCytM preserved a well-oxidized electron transport chain under photomixotrophy. Similarly, the triple mutant ΔCox/Cyd/CytM demonstrated high Y(II) compared to ΔCox/Cyd under photomixotrophy (Supplemental Fig. S7C-D, S8C-D).

To determine how WT builds up a highly reduced Q_A over three days of photomixotrophic growth, we monitored the redox kinetics of the PSII primary electron acceptor Q_A (Fig. 4) by firing a single-turnover saturating flash on dark-adapted cells. Relaxation of the chl fluorescence yield was then recorded in the period of subsequent darkness. No difference was observed between WT and ΔCytM cells cultured photoautotrophically (Supplemental Fig. S9A) and on the first day of photomixotrophy, both WT and ΔCytM cells demonstrated typical flash-fluorescence relaxation in the darkness. On the second day, WT cells demonstrated a substantial slow-down in Q_A^- re-oxidation reflected by slow decay kinetics (Fig. 4B), while on the third day, there was a nearly complete loss of Q_A-to-Q_B electron transfer (Fig. 4C).

Interestingly, the kinetics from the third day resembled a curve recorded in photoautotrophically cultured WT supplemented with DCMU prior to the measurement (Supplemental Fig. S9A). This supports the conclusion that Q_A-to-Q_B electron transfer was strongly inhibited in the majority of PSII centers in WT on the third day of photomixotrophy. Pre-illumination of the cells with far-red light did not accelerate Q_A^- re-oxidation (Supplemental Fig. S9B), thus supporting the idea that the inhibition is not simply due to a highly reduced PQ-pool, although over-reduction of the PQ-pool cannot be excluded.

ΔCox/Cyd and ΔCox/Cyd/CytM displayed pronounced waving in the fluorescence yield relaxation kinetics (Fig. 4 A-C). The wave phenomenon is an unusual pattern in the decay of flash-induced chl fluorescence yield in the dark. The feature is characterized by a dip, corresponding to transient oxidation of Q_A^-, and a subsequent rise, reflecting re-reduction of the PQ-pool by NDH-1 (Deák et al., 2014). During growth over the three-day period, the wave phenomenon in ΔCox/Cyd became less evident due to gradual inhibition of Q_A-to-Q_B electron transfer. In contrast, ΔCox/Cyd/CytM displayed prominent waving during all three days of photomixotrophic growth, demonstrating that Q_A^- re-oxidation was being sustained. Slight waving in ΔCox/Cyd under photoautotrophic conditions was reported previously (Ermakova et al 2016), and here we demonstrate that glucose induces a strong wave phenomenon.

In order to evaluate electron transfer through Cyt b_6f, the redox kinetics of Cyt *f* were examined (Fig. 5). Both photoautotrophically grown WT (Fig. 5A) and ΔCytM (Supplemental Fig. S10) demonstrated the fast oxidation of Cyt *f* followed by its reduction and re-oxidation, exhibiting wave-like kinetics upon dark-to-light transition. In the subsequent dark, rapid reduction of Cyt *f* was observed. When DCMU was added to WT prior to the measurement (Fig. 5A), illumination initiated steady oxidation but the transient re-reduction was eliminated and the subsequent reduction in dark was slower. Photomixotrophically grown WT (Fig. 5B) demonstrated trends similar to the DCMU-treated WT cells grown under photoautotrophic conditions, confirming that electron transfer from PSII to Cyt b_6f is inhibited. In contrast, ΔCytM grown photomixotrophically (Fig. 5B) resembled untreated WT cells subjected to photoautotrophic conditions.

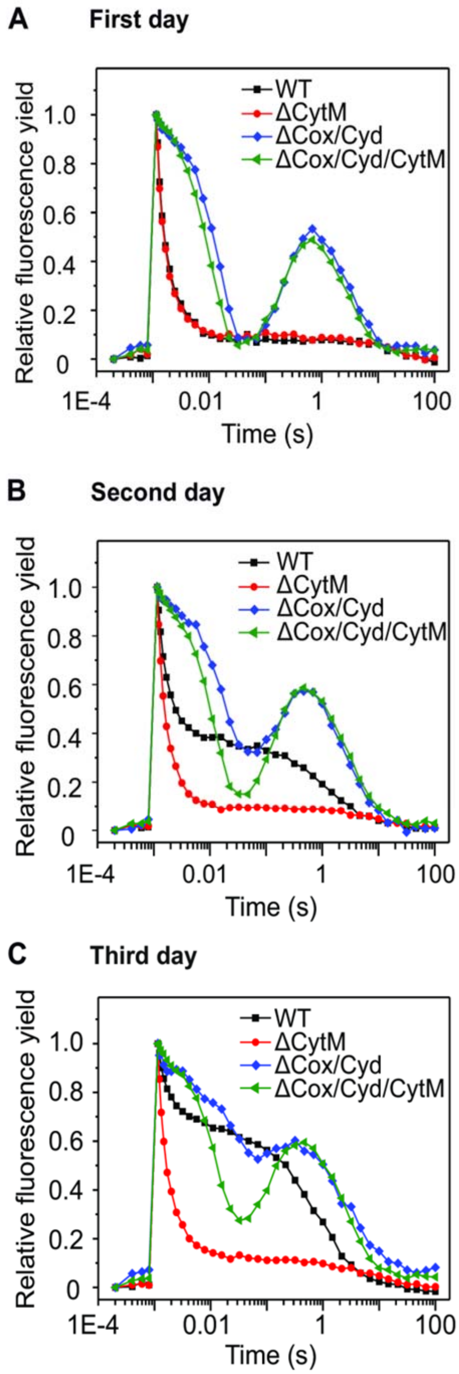

Figure 4. Relaxation of flash-induced fluorescence yield in cells exposed to darkness. Subsequent relaxation of fluorescence yields in the dark was measured after a single-turnover saturating pulse in photomixotrophically cultured cells taken on the first (A), second (B), and third day (C) of cultivation. Growth conditions are described in Fig. 3. Prior to measurements, the cell suspension was adjusted to 5 µg chl ml^{-1}, resuspended in BG-11 supplemented with 10 mM glucose (C, D), and dark adapted for 5 min.

These results demonstrate that during photomixotrophic growth, the electron flow at PSII acceptor site gradually becomes inhibited in WT leading to drastically slower electron transfer from PSII to Cyt b_6f on the third day. Deletion of CytM circumvents this inhibition, maintains PSII reaction center protein D1 amounts and a steady electron flux from PSII to Cyt *f*.

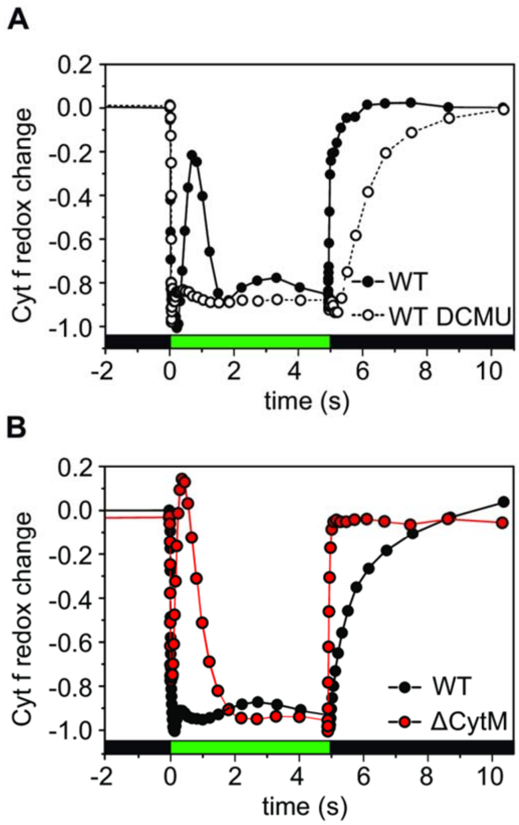

Figure 5. Redox kinetics of Cyt *f* in WT and ΔCytM cells. Cells were grown for three days under photoautotrophic (A) and photomixotrophic (B) conditions as described in Fig 3. Oxidation of Cyt *f* was induced by 500 μmol photons m^{-1} s^{-1} green light. When indicated, 20 μM DCMU was added prior the measurement. The curves were normalized to their respective maximal oxidation. The kinetics are representatives of three biological replicates.

ΔCytM has a larger pool of oxidizable PSI than WT under photomixotrophy

Next, we determined activity of PSI by monitoring the redox kinetics of P700, the primary electron donor of PSI (Fig. 6), which was performed simultaneously with chl fluorescence measurements (Fig. 3). First, the maximal amount of oxidizable P700, P_m, was determined (Fig. 6A). Compared to cells cultured under photoautotrophic conditions, WT cells grown photomixotrophically had 45.2±0.03% lower P_m. However, the difference between ΔCytM cultured under photomixotrophic and photoautotrophic conditions was negligible (17.2±19.3%). Thus, under photomixotrophic conditions, ΔCytM had 132±18.7% higher maximum amounts of oxidizable P700 than WT (Fig. 6A). In line with this, immunoblotting revealed higher levels of PSI reaction center subunit, PsaB, in ΔCytM compared to WT under photomixotrophic growth (Fig. 6B). To determine the PSI:PSII ratio, samples were analysed at 77K by measuring chl fluorescence emission. No statistical difference was observed between WT and ΔCytM (Supplemental Fig. S11), demonstrating that the PSII:PSI ratio was similar in both strains.

The PSI effective yield Y(I), was also quantified, and was three times lower in photomixotrophically cultured WT cells compared to those grown photoautotrophically (Supplemental Fig. S5B). This is due to a strong donor side limitation of PSI Y(ND) (Supplemental Fig. S5C), which demonstrates an electron shortage to $P700^+$. In contrast,

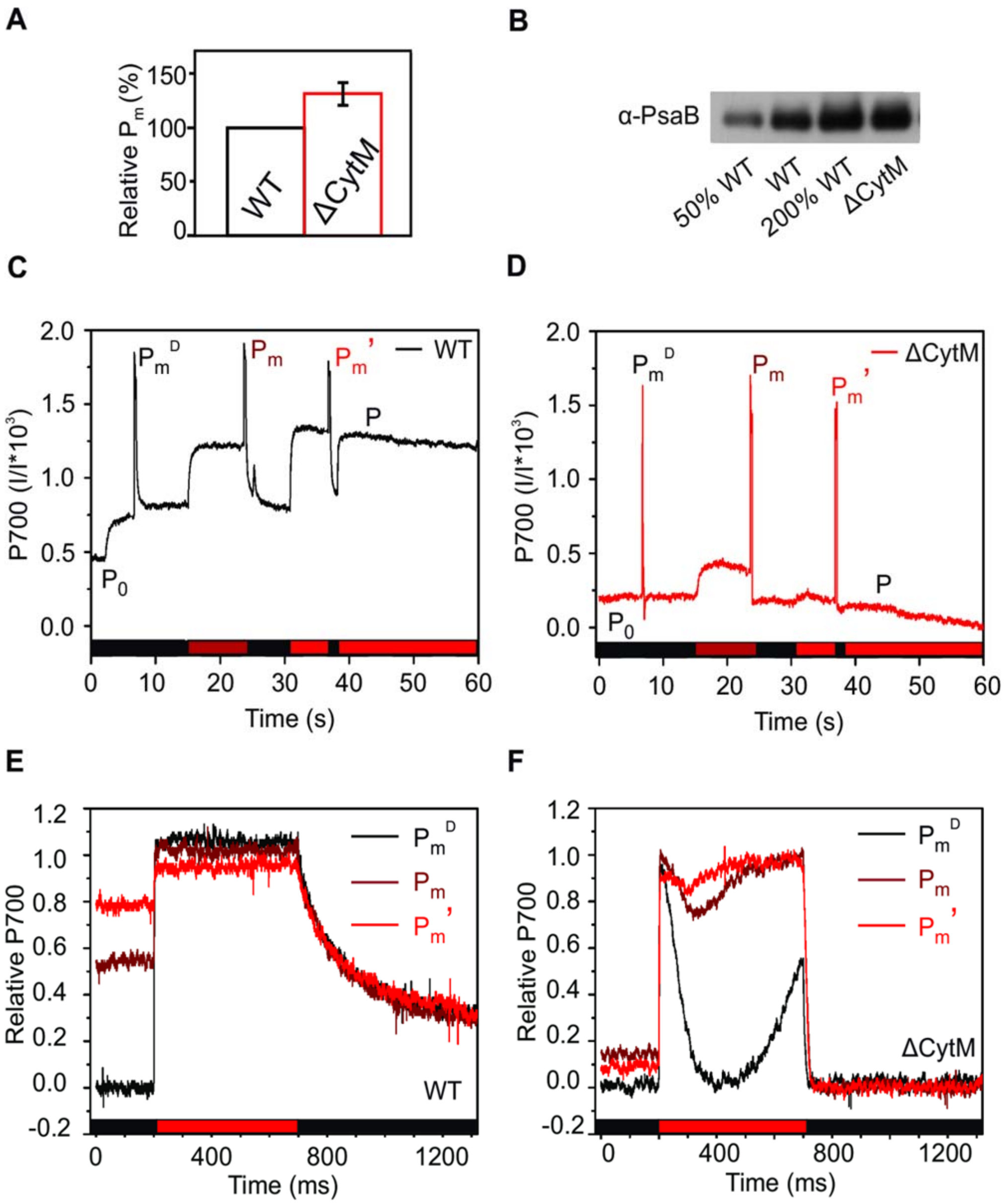

Figure 6. Characterization of PSI in cells cultured photomixotrophically. The maximal amount of oxidizable P700, P_m, (A) and immunoblotting of PSI reaction center protein, PsaB (B), was determined in cells cultured photomixotrophically. Values are means ± SD, n = three biological replicates. P700 oxidoreduction slow (C, D) and fast kinetics (E, F) were measured in parallel with fluorescence (Fig. 3). Fast kinetics curves (E, F) are normalized to P_m and referenced against their respective minimum P700 signal detected after the pulse. Cultivation, sample preparation, and experimental parameters are similar to those detailed in Fig. 3. P_0, initial P700; P_m^D, maximum P700 in darkness; P_m, maximum P700 under far-red light; P_m', maximum P700 under red actinic light.

photomixotrophically cultured ΔCytM demonstrated similar Y(I) and only slightly increased Y(ND) compared to photoautotrophically cultured WT and ΔCytM (Supplemental Fig. S5B, C). As a result, ΔCytM had more than three times higher Y(I) than WT under photomixotrophy (Supplemental Fig. S5B).

Next, pulse-induced P700 fast kinetics were compared between photoautotrophically and photomixotrophically cultured WT (Fig. 6E) and ΔCytM (Fig. 6F). These fast kinetics reveal the dynamics of P700 oxidoreduction during saturating pulses on millisecond scale. Saturating pulses are flashed in darkness (P_m^D) under far-red light (P_m) and actinic red light (P_m'). Typically, photoautotrophically cultured WT (Supplemental Fig. S12A) demonstrates transient $P700^+$ re-reduction during light pulses. However, photomixotrophically grown WT did not exhibit the typical transient re-reduction (Fig. 6E). Importantly, $P700^+$ relaxation after the pulse (Fig. 6E) was markedly slower compared to that observed in photoautotrophically cultured cells (Supplemental Fig. S12A). Collectively, these results confirm that fewer electrons were transferred to $P700^+$, leading to higher Y(ND) in photomixotrophically grown WT. Photomixotrophically cultured ΔCytM (Fig. 6F) displayed transient re-reduction during the pulses (see P_m^D, P_m^{FR} and P_m' on Fig. 6F) and rapid relaxation after the pulse (Fig. 6F), resembling photoautotrophically cultured ΔCytM and WT (Supplemental Fig. S12A-B).

Here, we have shown that the effective yield of PSI in photomixotrophically cultured WT cells was considerably lower compared to photoautotrophically cultured cells, due to an electron shortage at $P700^+$. This phenotype is eliminated by deleting *cytM*, as increased Y(I), higher amounts of oxidizable P700 (P_m) and PsaB were observed in ΔCytM compared to WT on the third day of photomixotrophy.

ΔCytM and ΔCox/Cyd/CytM sustain efficient net photosynthesis and CO_2 fixation under photomixotrophy

To analyse real time gas exchange in photomixotrophically grown WT, ΔCytM, ΔCox/Cyd, and ΔCox/Cyd/CytM (Fig. 7), whole cell fluxes of O_2 and CO_2 were simultaneously monitored using membrane inlet mass spectrometry (MIMS). In contrast to a classical oxygen electrode which only determines net O_2 changes, MIMS via enrichment of the samples with the stable $^{18}O_2$ isotopologue makes it possible to simultaneously measure the rates of gross $^{16}O_2$ production by PSII, and $^{18}O_2$ consumption mediated by flavodiiron proteins (Flv1-to-Flv4) and RTOs (Ermakova et al., 2016; Santana-Sanchez et al., 2019). Net O_2 fluxes were calculated by finding the difference between gross rates of $^{16}O_2$ production and $^{18}O_2$ consumption. Further, light-induced O_2 consumption was calculated by subtracting the rates of $^{18}O_2$ consumption in the dark from $^{18}O_2$ consumption in the light.

Although Rubisco fixes CO_2, and the instrument can only measure the concentration of CO_2 in a sample, cells consume both CO_2 and HCO_3^- from the medium. The pH-dependent equilibrium between CO_2 and HCO_3^- makes it possible to calibrate the CO_2 concentration measured with the MIMS to the total inorganic carbon (TC_i) concentration in the sample. Based on the assumption that during steady state photosynthesis the consumption of TC_i is a function of Rubisco activity (Badger et al., 1994; Sültemeyer et al., 1995), the TC_i fluxes represents CO_2 consumption rates.

In WT under 200 µmol photons m^{-2} s^{-1} white light, O_2 consumption and gross production rates were similar, resulting in nearly zero net photosynthetic O_2 production. This is in line with the data obtained by the O_2 electrode (Fig. 3E). Corresponding to the minor net photosynthetic O_2 production observed, the rate of CO_2 consumption was negligible (Fig. 7A;

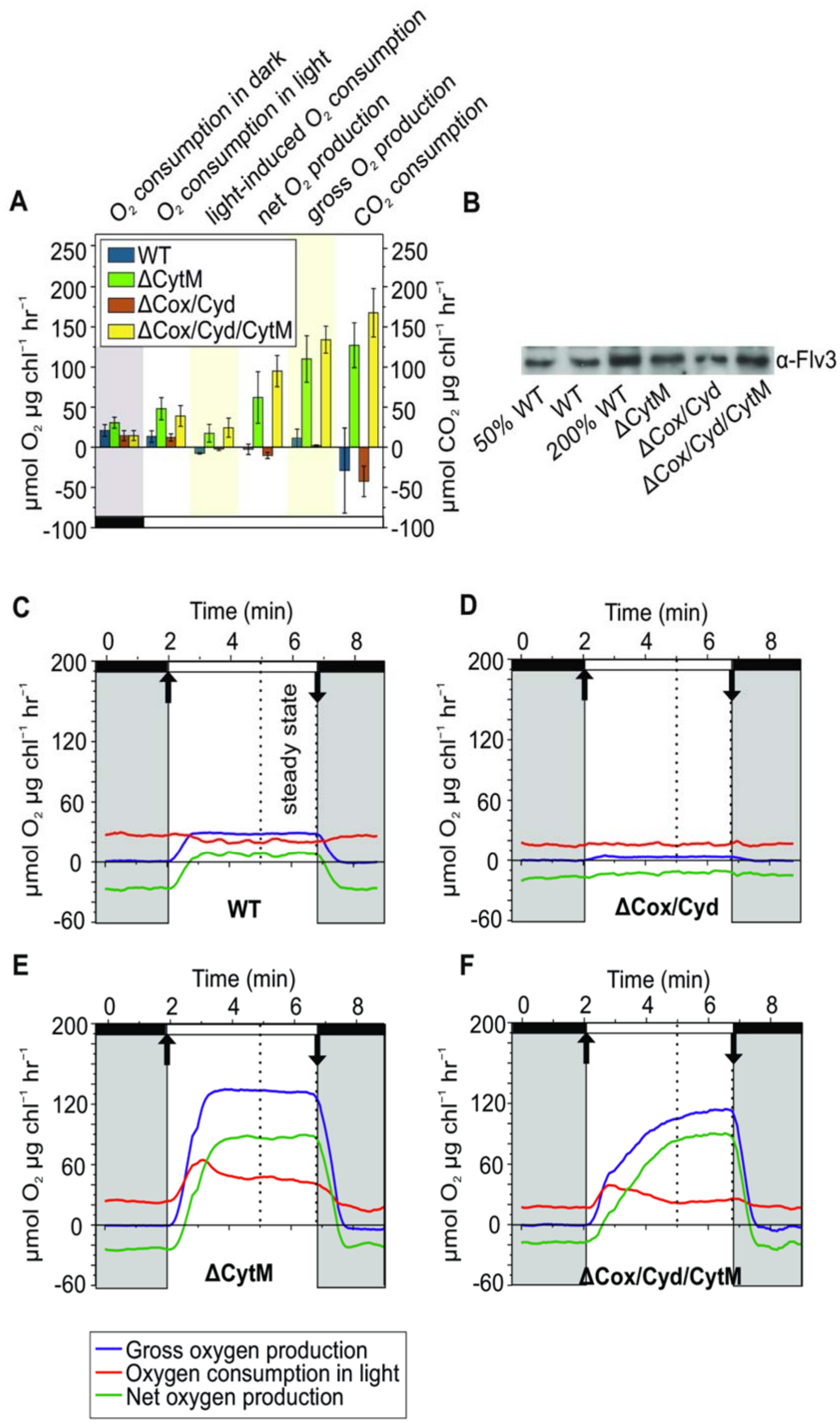

Figure 7. O_2 and CO_2 fluxes in photomixotrophically cultured WT, ΔCytM, ΔCox/Cyd, and ΔCox/Cyd/CytM cells. Rates of O_2 and CO_2 fluxes in steady state (A). Values are means ± SD, n = 3-5 biological replicates. Total protein extracts were analyzed by immunoblotting with *α*-Flv3-specific antibody (B). 15 µg total protein was loaded per 100% lane, 50% and 200% correspond to 7.5 µg and 30 µg, respectively. Kinetics of O_2 flux rates in whole cells (C-F). Cultivation, sample preparation, and experimental conditions are detailed in Fig. 3. In the light phase, 200 µmol photons m^{-2} s^{-1} constant white light was applied. Samples are supplemented by 1.5 mM $NaHCO_3$. Kinetics are representatives of 3-6 biological replicates. The source data of Fig. 7A can be found in Supplemental Table S2.

Supplemental Fig. S13A). Importantly, no light-induced O_2 consumption was observed in WT (Fig. 7A, C), although a substantial amount of Flv3 was detected by immunoblotting (Fig. 7B). While the thylakoid-localized RTOs, Cox and Cyd, were shown to be active in light (Ermakova et al., 2016), a slight inhibition of respiratory O_2 consumption under 200 µmol photons m^{-2} s^{-1} illumination occurred in WT. In contrast, ΔCytM exhibited a positive net O_2 production rate and active CO_2 consumption (Fig. 7A, E; Supplemental Fig. S13C). Strikingly, gross O_2 production was approximately 10 times higher compared to WT and $^{18}O_2$ consumption in light followed a triphasic pattern, a characteristic trend reflecting the contribution of Flv1/3 and Flv2/4 to O_2 consumption in light (Santana-Sanchez et al., 2019). The triphasic pattern in ΔCytM was observed as an initial burst of O_2 consumption following the dark-to-light transition, which faded after 1-1.5 min and continued at a relatively constant rate (Fig. 7E). Accordingly, immunoblotting confirmed higher accumulation of the Flv3 proteins in ΔCytM. The rate of light-induced O_2 consumption in ΔCytM is comparable to the reported values of photoautotrophically grown WT (Huokko et al., 2017, Santana-Sanchez et al., 2019). The dark respiration rate was slightly higher in ΔCytM compared to WT, as previously observed when ΔCytM was cultured under dark, heterotrophic conditions (Hiraide et al 2015).

Similar to WT, ΔCox/Cyd (Fig. 7A,D) showed minimal photosynthetic activity on the third day of photomixotrophic growth. During illumination, net O_2 production remained negative, and CO_2 consumption was found to be negligible (Fig. 7A, Supplemental Fig. S13B). Only residual gross O_2 production was observed and O_2 consumption was not stimulated by light (Fig. 7A, D). Flv3 protein abundance in ΔCox/Cyd was comparable to WT (Fig. 7B). In sharp contrast to ΔCox/Cyd, ΔCox/Cyd/CytM demonstrated high PSII activity and a net O_2 production rate similar to ΔCytM (Fig. 7A, F). ΔCox/Cyd/CytM displayed a triphasic O_2 consumption pattern under illumination (Fig. 7F) and the light-induced O_2 consumption was comparable to that of ΔCytM in steady state (Fig. 7E). Compared to ΔCox/Cyd, ΔCox/Cyd/CytM had higher levels of Flv3 (Fig. 7B). Notably, deleting *cytM* in the ΔCox/Cyd mutant did not enhance dark respiration, whereas ΔCytM had higher rates compared to WT.

To conclude, mutants lacking CytM sustained a steady electron flux towards O_2 and CO_2 under photomixotrophy, reflected by substantial net O_2 production and active CO_2 consumption during illumination.

Photomixotrophically cultured ΔCytM cells accumulate transport proteins and cofactor biosynthetic enzymes

In order to understand the metabolism of photomixotrophically grown WT and ΔCytM, we analysed the total proteome by nLC-ESI-MS/MS via the data-dependent acquisition (DDA) method. Samples for analysis were collected on the second day, when both WT and ΔCytM cells were in late exponential phase and a substantial ~~significant~~ growth difference was observed between the strains (Fig. 8A).

In total, 2,415 proteins were identified (Supplemental Dataset S1), despite the fact that the dataset was slightly biased against basic (Fig. 8D) and hydrophobic proteins (Fig. 8E), which is a known issue with this technique (Chandramouli and Qian, 2009). Out of 2,415 proteins, 634 were quantified, with 162 displaying a statistically different abundance in ΔCytM compared to WT (fold change (FC) >1.5 and FC < -1.5 ($P<0.05$)) (Supplemental Dataset

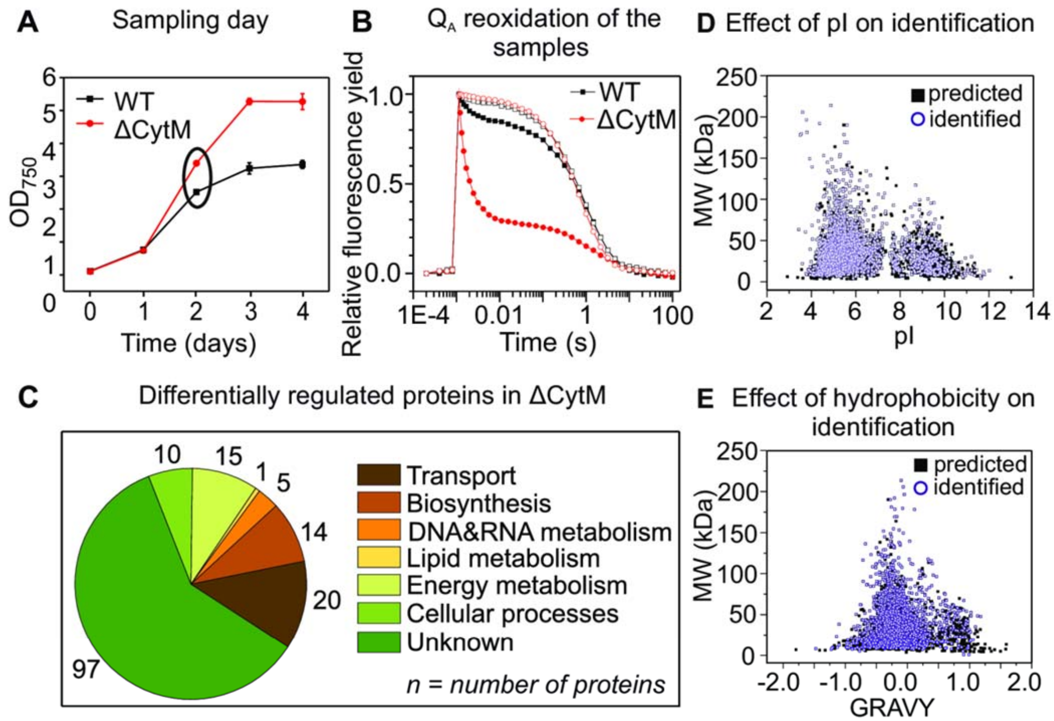

Figure 8. Characteristics at the sampling stage and functional classification of differentially regulated proteins in ΔCytM. Growth of the analysed cultures (A), with the ellipsis marking the sampling day. Cells were cultured similarly to those used in the biophysics analysis, except that the cells for proteomics were pre-cultivated under atmospheric CO_2 in order to fully adapt the cells to these conditions. Importantly, the extra pre-culturing step did not affect the growth of the experimental cultures. Values are means ± SD, n = 2 biological replicates. Relaxation of the flash-induced fluorescence yield in the dark (B) was measured in the absence (closed symbols) and in the presence of 20 µM DCMU (open symbols). Differentially regulated proteins in ΔCytM were grouped according to their function (C). In total, 2415 proteins were identified, out of which 634 proteins were quantified and 162 were differentially regulated. The practical significance of differentially regulated proteins was set to fold change (FC) > 1.5 and FC < -1.5 (ANOVA $p < 0.05$). Effect of isoelectric point (pI) (D) and hydrophobicity (GRAVY) (E) of the proteins on the identification rate was determined. Black squares mark all of the 3507 predicted proteins in Synechocystis, lilac circles mark each protein identified in WT and in ΔCytM.

S2). The functional classification of differentially regulated proteins (Fig. 8C) revealed that apart from unknown or hypothetical proteins, mainly transporters and biosynthetic enzymes were altered in photomixotrophically cultured ΔCytM cells.

Supplemental Dataset S3 shows a selection of proteins whose abundance was different in ΔCytM compared to WT. The highest fold change was observed in transport proteins. Among these, the constitutive low-affinity ABC-type phosphate transporters (PstA1, PstB1, PstB1', PstC), periplasmic P_i-binding proteins (SphX, PstS1), and extracellular lytic enzymes (PhoA, NucH) are more abundant in ΔCytM. Among proteins related to C_i uptake, a thylakoid *β*-type carbonic anhydrase, EcaB, was 2.32 times (P = 7.50E-03) more abundant in ΔCytM. EcaB is a CupA/B-associated protein, proposed to regulate the activity of NDH-1_3 (NDH-1 MS) and NDH-1_4 (NDH-1 MS') (Sun et al., 2018). NDH-1_3 facilitates inducible CO_2-uptake, whereas NDH-1_4 drives constitutive CO_2-uptake (Ogawa, 1991). CupB is exclusively found in the NDH-1_4 complex and converts CO_2 into HCO_3^-. Interestingly, no significant change was observed in the level of the glucose transporter GlcP, although the growth advantage of ΔCytM was observed upon exposure to glucose.

Chl *a* biosynthetic enzymes were found to accumulate in the mutant (Supplemental Dataset 3). ChlL, a subunit of the light-independent protochlorophyllide reductase (Wu and Vermaas 1995), and ChlP (4.61E-03), a geranylgeranyl reductase (Shpilyov et al., 2005), were 9.28 fold (P = 5.32E-03) and 1.52 fold (P = 4.61E-03) upregulated in ΔCytM, respectively. The incorporation of chl into photosystems likely increases due to the elevated level of Pitt, a protein contributing to the formation of photosynthetic pigments/proteins at the early stages of biogenesis (Schottkowski et al., 2009). The ligand of the tetrapyrrole ring of chl is Mg^{2+} and accordingly, the magnesium uptake protein MgtE accumulated in ΔCytM along with a periplasmic iron-binding protein, FutA2, part of the complementary uptake-system of iron, a vital element of the photosynthetic machinery (Kranzler et al., 2014). Among pigment biosynthetic enzymes, ΔCytM showed increased levels of the heme oxygenase Ho1, catalysing the final step in the production of biliverdin (Willows et al., 2000). Biliverdin is the precursor of phycocyanobilin, which is incorporated into phycobilisomes, the light-harvesting complexes of Synechocystis.

Among the photosynthetic proteins, the PSI reaction center subunit PsaB was found in equal amounts in WT and ΔCytM. However, immunoblotting with an anti-PsaB antibody demonstrated that ΔCytM contained higher amounts of PsaB than WT (Fig. 6B). This discrepancy may be due to the fact that despite the robustness of the MS-based DDA method, hydrophobic membrane proteins are prone to misquantification. Via MS analysis, quantification of *psbA* encoded D1 was not successful. Therefore, its abundance was only determined by immunoblotting (Fig. 3F), which revealed higher levels of D1 proteins in ΔCytM compared to WT. Interestingly and somewhat contradictorily, the amount of PSII assembly proteins encoded by the PAP-operon (Wegener et al., 2008) decreased in the mutant. We also note that lower levels of NorB, a quinol-oxidizing nitric oxide reductase (Büsch et al 2002), were observed in ΔCytM.

Since the growth advantage of ΔCytM was observed in the presence of glucose, alterations are expected in the abundance of the intermediary carbon metabolic enzymes. In Synechocystis, roughly 100 enzymes participate in this metabolic network. In our study, 40 were quantified and surprisingly, only a few proteins were differentially regulated in ΔCytM. One notable example is phosphofructokinase PfkA, the key regulatory enzyme of the glycolytic Embden–Meyerhof–Parnas pathway, which was 1.86 times (P = 1.96E-05) less abundant in ΔCytM, suggesting that carbon flux might be redirected into the Entner–Doudoroff or oxidative pentose phosphate pathways. Phosphoglycerate kinase Pgk, which is involved in each glycolytic pathway, was 2.06 times (P = 1.27E-05) as abundant in ΔCytM. Phosphoenolpyruvate synthetase PpsA, a protein that catalyses the first step of gluconeogenesis, was 2.21 times (P = 3.10E-04) less abundant in ΔCytM.

To conclude, global proteomic analysis revealed that photomixotrophically cultured ΔCytM accumulates transporter and chl biosynthetic proteins, while slight changes in the amount of certain glycolytic and photosynthetic proteins were also observed.

Discussion

The effect of importing and metabolising organic carbon on the bioenergetics properties of cyanobacteria over a long-term period is not fully understood. Previous studies have focused on the cellular changes following relatively short-term (from 10 min to 24 h) exposure to organic carbon (Lee et al., 2007; Takahashi et al.. 2008; Haimovich-Dayan et al., 2011; Zilliges and Dau, 2016). The majority of these reports suggest partial inhibition of photosynthetic activity, whereas some studies demonstrated increased net photosynthesis under air-level CO_2 after 2 h exposure to 10 mM glucose (Haimovich-Dayan et al., 2011). However, long-term changes to bioenergetics processes, particularly photosynthesis, remain to be elucidated. In this study, we investigated the effect of long-term photomixotrophic growth on WT and ΔCytM cells, most notably on the photosynthetic machinery, by analysing chlorophyll fluorescence, the redox kinetics of P700, real time O_2 and CO_2 fluxes, and changes within the proteome.

Gradually disconnecting PSII from Cytb_6*f* limits photosynthesis in photomixotrophically cultured WT

By characterizing WT cells shifted from photoautotrophic to photomixotrophic conditions, we show that photosynthesis was markedly decreased over three days of cultivation. This is deduced from the low PSII (Fig. 3C; Supplemental Fig. S5A) and PSI yield (Fig. 6C, Supplemental Fig. S5B) and most importantly, the negligible net O_2 production (Fig. 3E) and CO_2 fixation rates (Fig. 7A, Supplemental Fig. S13A) on the third day. A residual PSII activity is ensured by circulating electrons in a water-water cycle. This was demonstrated by reduced PSII gross O_2 production (Fig. 7A, C) which nearly equalled O_2 consumption in the light, resulting in practically zero net O_2 production. Since addition of an artificial PSII electron acceptor, DCBQ, largely restores O_2 evolving activity (Fig. 3E), a ~~significant~~ substantial portion of PSII centers are functional, but downstream electron flux is restricted. This could be due to a highly reduced PQ-pool, which in turn affects redox potential of Q_B thus Q_A^- re-oxidation (Haimovich-Dayan et al., 2011). However, far-red light which specifically excites PSI and drains electrons from the PQ-pool did not accelerate Q_A^- re-oxidation in photomixotrophically cultured WT (Supplemental Fig. S9B). Thus, over-reduction of the PQ-pool cannot be the sole reason for the restricted downstream electron flux. Interestingly, photomixotrophically cultured WT resembles DCMU-treated cells in many ways: (i) far-red light illumination increases steady state fluorescence (Fig. 3C, Supplemental Fig. S4); (ii) transient re-reduction and subsequent re-oxidation of Cyt *f* under illumination is nearly absent and Cyt *f* decay in darkness is slow (Fig. 5); (iii) flash-induced decay of Q_A^- after 3 days exposure to glucose highly resembles the kinetics of DCMU-treated cells (Fig. 8B) and differs from kinetics observed in DBMIB-treated WT (Supplemental Fig. S9B; et al 2014). These results suggest that photosynthetic electron flow from PSII to PQ-pool and Cyt b_6f is hindered. However, this is not simply due to a highly reduced PQ pool.

The gradual disconnection between PSII and Cyt b_6f and resulting decrease in photosynthesis could be due to a spatial isolation of PSII via rearrangement in the thylakoid to another location. Rearrangement of thylakoid-localised complexes, specifically NDH-1 and SDH, has been observed in response to redox-regulated changes in the electron transport chain (Liu et al 2012). Applying the same analogy to PSII, the highly reduced state of the PQ-pool might trigger the complexes to arrange into a more sparse distribution during photomixotrophic growth. Although cyanobacterial thylakoids are densely packed membranes (Kaňa et al., 2013), lateral heterogeneity (Agarwal et al., 2010) and mobility of PSII (Casella et al., 2017) has been previously demonstrated.

Photomixotrophy does not alter photosynthetic electron transport in ΔCytM

Surprisingly, deletion of CytM reverses the downregulation of photosynthesis in photomixotrophy, resulting in a profile similar to WT and ΔCytM cells grown under photoautotrophic conditions. Importantly, ΔCytM demonstrated unrestricted electron flow between PSII, Cyt b_6f, and PSI. The rate of gross O_2 production (Fig 7A, E) was ten times higher in ΔCytM than it was in WT cells cultured under photomixotrophic conditions. Contrary to photomixotrophically cultured WT, ΔCytM showed a clear wave-pattern in Cyt *f* kinetics upon dark-to-light transition and did not demonstrate slow re-reduction of Cyt *f* in dark (Fig. 5B) or PSI donor-side limitation (Supplemental Fig. S5C). Finally, the abundance of D1 (Fig. 3F), PsaB (Fig. 6B), and PetA and PetB (Supplemental Dataset S3), the core subunits of PSII, PSI, and Cyt b_6f, respectively, was higher in ΔCytM than in WT, although the PSI:PSII ratio was unaltered (Supplemental Fig. S11). As a consequence, the rate of net O_2 production and CO_2 consumption (Fig. 7A) was substantially higher in ΔCytM, demonstrating that deletion of CytM conserves photosynthetic activity and circumvents the inhibition of Q_A^- re-oxidation in photomixotrophy.

The exact mechanism by which ΔCytM alleviates blockage of the electron transport pathway was not elucidated in this work, nor has an exact role for this protein been determined in previous studies. CytM has been suggested to play a role in transferring electrons from Cyt b_6f to Flv1/3, limiting productivity but providing a possible alternative route for safely transferring electrons to O_2 (Hiraide et al., 2015). However, given the low midpoint potential of CytM, a large energy barrier would have to be overcome in order for electron transfer downstream of Cyt b_6f to occur (Cho et al., 2000). Moreover, we demonstrated that the absence of CytM does not decrease O_2 photoreduction driven by FDPs in ΔCox/Cyd/CytM (Fig. 7A, F), thus excluding this possibility. Recently, a cyanobacterial ferredoxin, Fed2, was shown to play a role in iron sensing and regulation of the IsiA antenna protein, a protein which is typically expressed when cells are exposed to low-iron conditions (Schorsch et al., 2018). Similar to Fed2, it is possible that CytM plays a regulatory role in the cell, rather than being directly involved in electron transport under photomixotrophy.

Under conditions when cells are exposed to glucose or other sugars, CytM may regulate carbon assimilation. ΔCytM demonstrates substantial growth under dark heterotrophic conditions (Hiraide et al., 2015). However, the majority of the known cyanobacteria cannot grow heterotrophically, indicating that the function of CytM extends beyond the modulation of heterotrophic growth (Bialek et al., 2016). Under photomixotrophic conditions, CytM likely is

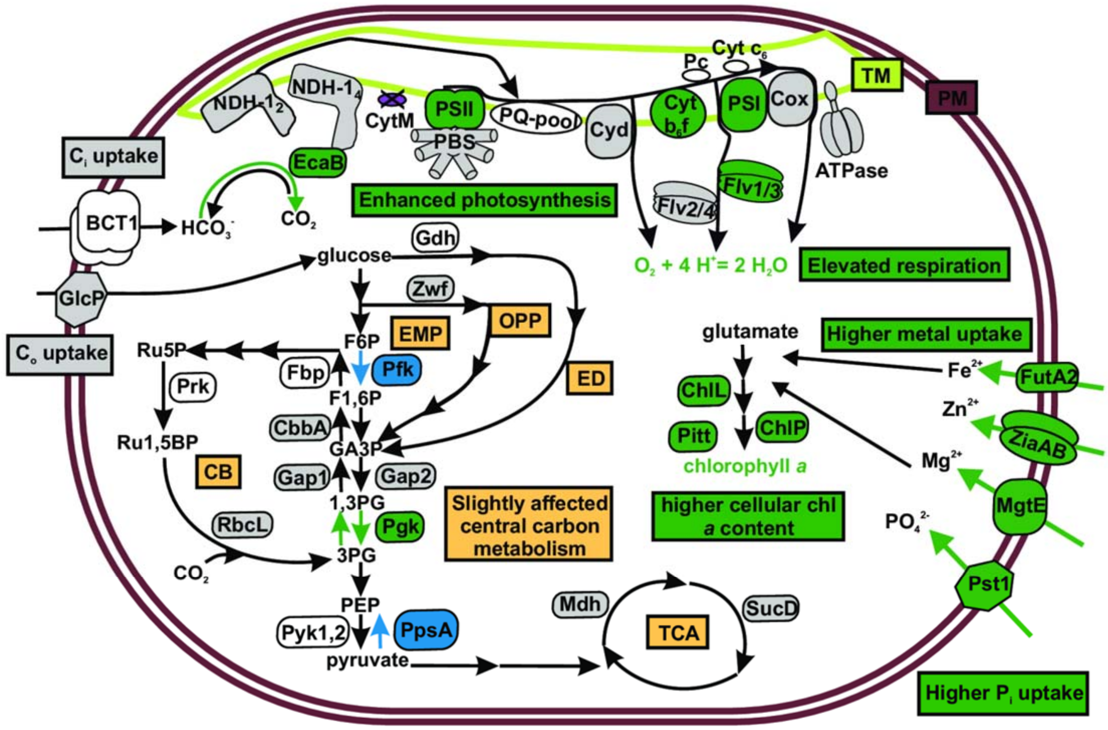

Fig. 9. Schematic showing changes in the metabolism in photomixotrophically grown ΔCytM cells compared to WT. Proteins, compounds, and metabolic routes with increased abundance or activity in ΔCytM relative to the WT are marked in green. Blue marks lower abundance in ΔCytM, grey marks unchanged, and white marks undetermined abundance or activity. TM, thylakoid membrane; PM, plasma membrane; C_i uptake, inorganic carbon uptake; C_o uptake, organic carbon uptake; EMP, Embden-Meyerhof-Parnas pathway; OPP, oxidative pentose phosphate pathway; ED, Entner-Doudoroff pathway; CB, Calvin-Benson cycle; TCA, tricarboxylic acid cycle; P_i uptake, inorganic phosphate uptake.

involved in regulation of thylakoid re-arrangements or photosynthetic electron transport and carbon fixation, limiting CO_2 uptake and decreasing the total amount of photosynthetic proteins, which in turn reduces photosynthesis. In line with this, we observed accumulation of EcaB in ΔCytM (Fig. 9; Supplemental Dataset S3). Enhanced EcaB levels likely results in greater inorganic carbon assimilation, higher carbon fixation, and increased turnover of NADPH, the terminal electron acceptor in linear photosynthetic electron transport. This in turn likely limits over-reduction of the photosynthetic electron transport chain.

Regardless of the exact role of CytM, it is clear that deletion of this protein substantially increases growth of Synechocystis in photomixotrophy (Fig. 1), in line with previous studies (Hiraide et al., 2015). This is possibly due to an increase in photosynthetic capacity combined with efficient assimilation of glucose into central metabolism, resulting in greater biomass accumulation. This resulted in increased production of proteins required for enhanced growth, including those involved in phosphate uptake (PstA1, PstB1, PstB1', PstC) (Supplemental Dataset S3), import of Mg^{2+} (MgtE), Zn^{2+} (ZiaA), and Fe^{2+} (FutA2), and production of chl (ChlP, ChlL) (Fig. 9; Supplemental Dataset S3).

In conclusion, under long-term photomixotrophy Synechocystis cells gradually decrease photosynthetic electron transport by disconnecting PSII from Cyt b_6f. Deletion of CytM allows Synechocystis to maintain efficient photosynthesis and enhanced growth under long-term photomixotrophy. While we have not determined the exact function of CytM, we propose that it plays a role in reducing photosynthesis under conditions when both light intensity and glucose concentration fluctuate (Hieronymi and Macke, 2010; Ittekkot et al., 1985), and the redox state of the intertwined photosynthetic and respiratory electron transfer rapidly changes.

Materials and methods

Plasmid construction

The genome sequence of Synechocystis (*Synechocystis* sp. PCC 6803) released 11.05.2004 was consulted via Cyanobase (http://genome.kazusa.or.jp/cyanobase) for primer design. Primers are listed in Supplemental Table S1. The *cytM* (*sll1245)* gene was deleted by amplifying a 906 bp fragment upstream of *cytM* using primers CytMleftfor and CytMleftrev and a 932 bp fragment downstream of *cytM* using primers CytMrightfor and CytMrightrev, followed by insertion of the respective fragments into the SacI/EcoR1 and XbaI/BamH1 sites of pUC19 to generate pCytM-1. The BamH1 digested npt1/sacRB cassette from pUM24Cm (Ried and Collmer, 1987) was inserted into the BamH1 site between the upstream and downstream fragments in pCytM-1 to generate pCytM-2.

Construction of *cytM* deletion mutants

Unmarked mutants of Synechocystis lacking *cytM* were constructed via a two-step homologous recombination protocol according to Lea-Smith et al., 2016. To generate marked mutants approximately 1 µg of plasmid pCytM-2 was mixed with Synechocystis cells for 6 hours in liquid media, followed by incubation on BG-11 agar plates for approximately 24 hours. An additional 3 mL of agar containing kanamycin was added to the surface of the plate followed by further incubation for approximately 1-2 weeks. Transformants were subcultured to allow segregation of mutant alleles. Segregation was confirmed by PCR using primers CytMf and CytMr, which flank the deleted region. To remove the *npt*1/*sacRB* cassette to generate unmarked mutants, mutant lines were transformed with 1 µg of the markerless CytM-1 construct. Following incubation in BG-11 liquid media for 4 days and agar plates containing sucrose for a further 1-2 weeks, transformants were patched on kanamycin and sucrose plates. Sucrose resistant, kanamycin sensitive strains containing the unmarked deletion were confirmed by PCR using primers flanking the deleted region (Supplemental Fig. S2B). The ΔCox/Cyd/CytM unmarked strain was generated via the same method in the background of the unmarked ΔCox/Cyd strain (Lea-Smith et al., 2013).

Cultivation

Cells kept in cryogenic storage were revived on BG-11 agar plates at 3% CO_2. Pre-experimental cultures were inoculated at 0.1 OD_{750} by transferring a patch of cells from plates into 30 ml BG-11 medium buffered with 10 mM TES-KOH (pH 8.2) in 100 ml Erlenmeyer flasks. Cultures were shaken at 120 rpm at 30°C and exposed to constant white fluorescent light of 50 µmol photons m^{-2} s^{-1} intensity in a Sanyo Environmental Test Chamber (Sanyo Co, Japan) which was saturated with 3% CO_2. Pre-experimental cultures were cultivated for three days with density typically reaching 2.5±0.5 OD_{750}.

Experimental cultures for growth and photophysiological experiments were inoculated in 30 ml fresh BG-11 media at 0.1 OD_{750} from harvested pre-experimental cultures. The media was buffered with 10 mM TES-KOH (pH 8.2), the CO_2 concentration was atmospheric, and cultures were agitated in 100 ml Erlenmeyer flasks at 120 rpm in AlgaeTRON AG130 cool-white LED chambers (PSI Instruments, Czech Republic). Growth was tested under constant light of 50 µmol photons m^{-2} with different glucose starting concentrations: (a) no glucose; (b) 5 mM glucose; and (c) 10 mM glucose. At 10 mM glucose, additional light regimes were tested: (d) 10 µmol photons m^{-2} s^{-1} light and (e) 15 min 50 µmol photons m^{-2} s^{-1} every 24 h. For photophysiological studies, cells were cultivated under condition (c) for three days. For proteomics analysis, cells were cultivated similarly to (c), with the exception of an extra three day long pre-cultivation step at atmospheric CO_2 without glucose.

Cell counting, cell size determination

Cell number was determined with a Nexcelom Cellometer X2 via the following method. Sample OD_{750} was adjusted to one, brightfield images were captured, and the cell number was determined by the Nexcelom software. In order to exclude the visual glitches falsely recognized as cells by the software, only the four most populous cell size groups were averaged. Typically, three thousand cells were counted per plate.

Glucose determination

Glucose concentration of the spent media was determined spectrophotometrically with the commercial High Sensitivity Glucose Assay Kit (Sigma-Aldrich, U.S.). Prior to measurements, the cell suspension was centrifuged at 5000 g for 10 min and the supernatant was filtered through a 0.2 µm filter.

MIMS measurements

Gas fluxes of intact cells were measured using membrane inlet mass spectrometry. The in-house built system consists of a DW-1 oxygen electrode chamber (Hansatech Ltd., U.K.) connected to the vacuum line of a mass spectrometer (Prima PRO model, Thermo Scientific, U.S.). The sample cuvette was separated from the vacuum line by a Hansatech S4 PTFE membrane (Hansatech Ltd., U.K.). Samples were pelleted and re-suspended in fresh BG-11 supplemented by 10 mM glucose and buffered to pH 8.2 with 10 mM TES-KOH. Chl *a* concentration was adjusted to 10 µg ml^{-1}. Prior to measurements, the sample was enriched with 98 % $^{18}O_2$ heavy isotope (CK Isotopes Limited, U.K.), the dissolved total inorganic carbon concentration was adjusted to 1.5 mM by adding $NaHCO_3$, and then 10-15 min dark adaptation was applied. The measurement was performed in a semi-closed cuvette at 30°C with constant stirring. The light source was a 150 Watt, 21 V, EKE quartz halogen-powered fiber-optic illuminator (Fiber-Lite DC-950, Dolan-Jenner, U.S.). A two-point calibration was used to calibrate the O_2 signal in milli-Q H_2O. Total inorganic carbon was calibrated by injecting known HCO_3^- samples into a known volume of growth media buffered to pH 8.2 with 10 mM TES-KOH. A mathematical offset accounted for the changing concentration of the $^{18}O_2$ and $^{16}O_2$ isotopologues over the course of an experiment to enable the accurate determination of rates (Hoch and Koch 1963) Rates were calculated as described previously (Beckmann et al 2009).

Clark-type electrode measurements

Net O_2 production of intact cells was tested in the presence of 0.5 mM 2,6-dichloro-*p*-benzoquinone (DCBQ) at 30°C with a Clark-type oxygen electrode and chamber (Hansatech Ltd., U.K.). Prior to the measurements, cells were resuspended in BG-11 (pH 8.2) supplemented with 10 mM glucose, the chl *a* concentration was adjusted to 7.5 μg ml^{-1}, then the samples were dark adapted for 1-2 min. O_2 production was initiated by 1,000 μmol photons m^{-2} s^{-1} white light using a Fiber-Lite DC-950 light source. Rates of oxygen production was calculated using the Hansatech software.

Chl fluorescence and P700 oxidoreduction measurements

Whole cell chl fluorescence was measured simultaneously with P700 with a pulse amplitude-modulated fluorometer (Dual-PAM-100, Walz, Germany). Prior to measurements, cells were resuspended in BG-11 (pH 8.2) supplemented with 10 mM glucose and the chl *a* concentration was adjusted to 15 μg ml^{-1}. Measurements were performed at 30°C, and samples were initially incubated in darkness for 15 minutes with stirring. To determine P_m, 30 s strong far-red light (720 nm, 40 W m^{-2}) and red multiple turnover saturating pulses (MT) were applied. MT pulses were set to an intensity of 5,000 μmol photons m^{-2} s^{-1} (width: 500 ms). Red (635 nm) actinic light was at an intensity of 50 μmol photons m^{-2} s^{-1} was used as background illumination. Photosynthetic parameters were calculated as described previously (Klughammer et al 2008 a,b).

Relaxation of flash-induced fluorescence yield was monitored using a fluorometer (FL3500, PSI Instruments, Czech Republic) as outlined previously (Allahverdiyeva et al 2003). Prior to the measurement, cells were resuspended in BG-11 (pH 8.2) supplemented with 10 mM glucose, adjusted to 5 μg chl *a* ml^{-1} and dark adapted for 5 min. Curves were normalized to F_0 and F_m.

Measurement of cytochrome *f* redox kinetics

Cyt *f* redox kinetics were determined in intact cells by deconvoluting absorbance changes at 546, 554, 563, and 573 nm that were measured using a JTS-10 pump probe spectrophotometer (BioLogic, Grenoble, France) and appropriate 10 nm FWHM interference filters. BG39 filters (Schott, Mainz, Germany) were used to shield the light detectors from scattered light. Deconvolution was performed with the JTS-10 software. Prior to the experiments, cells were harvested and Chl *a* concentration was adjusted to 5 μg ml^{-1} by resuspension in fresh BG-11 with or without 10 mM glucose. Cells were dark-adapted for 2 min prior to measurements with each interference filter, and then illuminated with 500 μmol photons $m^{-2}s^{-1}$ of green light for 5 s. Flashes of white detection light were administered during 200 μs dark intervals in actinic illumination. When appropriate, 20 μM DCMU was added to the samples before dark-adaptation.

Western blotting

Total protein extraction, electrophoresis and immunoblotting was performed as described previously (Huokko et al., 2019). Antibodies raised against PsaB (Agrisera, Vännäs, Sweden, AS10 695), D1 (Agrisera, Vännäs, Sweden, AS11 1786) and Flv3 (Antiprot, Puchheim, Germany) were used in this study.

MS analysis: sample preparation, data-dependent analysis, protein identification and quantitation

For data analysis, we used the proteome of *Synechocystis* sp. 6803 substr. Kazusa sequenced in 2004. Protein annotation was downloaded from Uniprot and Cyanobase. Hydrophobicity was determined via the GRAVY (grand average of hydropathy) index at www.gravy-calculator.de and pI was calculated via https://web.expasy.org/compute_pi/.

Sample preparation for MS, data-dependent analysis, and protein identification was performed as detailed previously (Huokko et al., 2019). The mass spectrometry proteomics data was deposited to the ProteomeXchange Consortium via the PRIDE (Perez-Riverol et al 2019) partner repository with the dataset identifier PXD015246 and 10.6019/PXD015246.

Statistical analysis

P values were calculated by one-way analysis of variance (ANOVA) technique and differences in the data were considered statistically significant when $P < 0.05$.

Accession numbers

Gene/protein names and accession numbers of all genes/proteins identified in this study are listed in Supplemental Dataset S1. The mass spectrometry proteomics data was deposited to the ProteomeXchange Consortium via the PRIDE (Perez-Riverol et al., 2019) partner repository with the dataset identifier PXD015246 and 10.6019/PXD015246.

Supplemental Data

Supplemental Figure S1. Alignment of CytM from sequenced cyanobacterial species.

Supplemental Figure S2. Generation of *cytM* deletion mutants in Synechocystis.

Supplemental Figure S3. Cell size of WT and ΔCytM grown photomixotrophically and photoautotrophically.

Supplemental Figure S4. Fluorescence transients of photoautotrophically cultivated WT and ΔCytM determined in the presence of 2 µM DCMU.

Supplemental Figure S5. Photosynthetic parameters of WT and ΔCytM grown photomixotrophically and photoautotrophically.

Supplemental Figure S6. Fluorescence transients and P700 oxidoreduction on the third day of photomixotrophic growth of the WT Synechocystis substrain.

Supplemental Figure S7. Fluorescence transients and P700 oxidoreduction kinetics of photomixotrophically grown WT, ΔCytM, ΔCox/Cyd, and ΔCox/Cyd/CytM.

Supplemental Figure S8. Fluorescence transients and P700 oxido-reduxtion kinetics of photoautotrophically grown WT, ΔCytM, ΔCox/Cyd, and ΔCox/Cyd/CytM.

Supplemental Figure S9. Flash-induced increase of fluorescence yield and its relaxation in dark in photoautotrophically grown WT and ΔCytM.

Supplemental Figure S10. Redox kinetics of Cyt *f* in photoautotrophically grown ΔCytM cells.

Supplemental Figure S11. 77K steady state fluorescence emission spectra of WT and ΔCytM grown photomixotrophically.

Supplemental Figure S12. Fast kinetics of P700 oxidoreduction of WT and ΔCytM grown under photoautotrophic conditions.

Supplemental Figure S13. The rate of CO_2 fluxes in photomixotrophically grown WT, ΔCytM, ΔCox/Cyd, and ΔCox/Cyd/CytM.

Supplemental Table S1. List of oligonucleotides used in this study.

Supplemental Table S2. Rates of O_2 and CO_2 fluxes in photomixotrophically grown WT, ΔCytM, ΔCox/Cyd, and ΔCox/Cyd/CytM.

Supplemental Dataset S1 Proteins identified by data-dependent analysis in photomixotrophically grown WT and ΔCytM.

Supplemental Dataset S2. Differentially expressed proteins in photomixotrophically grown ΔCytM versus WT.

Supplemental Dataset S3. A selection of differentially expressed proteins in photomixotrophically cultured ΔCytM compared to WT.

Acknowledgements

We thank Steffen Grebe for helping with Dual-PAM measurements and Ville Käpylä for laboratory assistance. MS analysis was performed at the Turku Proteomics Facility hosted by University of Turku and Åbo Akademi University, supported by Biocenter Finland. This work was supported by the Academy of Finland (project #315119 to Y.A. and the Finnish Center of Excellence, project #307335), the NordForsk Nordic Center of Excellence ‘NordAqua’ (#82845), and the Waste Environmental Education Research Trust (C.J.H.).

Figure legends

Figure 1. Impact of different glucose concentrations and light regimes on the growth of wild type (WT), ΔCytM, ΔCox/Cyd, and ΔCox/Cyd/CytM. Cultures were exposed to 50 μmol photons m^{-2} s^{-1} light (A, B) and were grown under photoautotrophic conditions without glucose (dash-dot-dot line) or under photomixotrophic conditions with 5 mM glucose (solid line) or 10 mM glucose (dashed line). Growth was then assessed under various light regimes in cultures containing 10 mM glucose (C, D), under constant 50 μmol photons m^{-2} s^{-1} light (dashed line), constant 10 μmol photons m^{-2} s^{-1} light (solid line) and light-activated heterotrophic growth (LAHG) which included 15 min of 50 μmol photons m^{-2} s^{-1} light exposure every 24 h (dash-dot-dot line). Values are means ± SD, n = 3-7 biological replicates.

Figure 2. Glucose consumption, cellular chl content, and cell number of WT and ΔCytM cultures on the third day of photomixotrophic growth. Amount of glucose consumed by the cells (A) was deduced from the remaining glucose in spent media on the third day. This number reflects the consumption of the whole culture rather than the glucose uptake rate of a given number of cells. Optical density per cell number (B) and cellular chl content (C) were determined. Values are means ± SD, n = three biological replicates. Cultures were grown photomixotrophically under constant 50 μmol photons m^{-2} s^{-1} illumination supplemented with 10 mM glucose. Samples were taken on the third day.

Figure 3. Fluorescence yield in WT and ΔCytM cells and quantification of O_2 production capacity during photomixotrophic growth. Chl fluorescence of photoautotrophically (A, B) and photomixotrophically (C, D) grown WT and ΔCytM whole cells. Photoautotrophic and photomixotrophic cultures were grown under constant 50 μmol photons m^{-2} s^{-1} illumination for three days, with or without 10 mM glucose, respectively. Prior to measurements, cells were resuspended in BG-11 supplemented with (C, D) and without (A,B) 10 mM glucose and dark adapted for 15 min. Maximum fluorescence was determined by applying a multiple turnover saturating pulse (500 ms, 5000 μmol photons m^{-2} s^{-1}) in darkness (black bars), under 40 W m^{-2} far-red light (brown bars) and under 50 μmol photons m^{-2} s^{-1} actinic red light (red bars). F_0, initial fluorescence; F_m^D, maximum fluorescence in dark; F_m^{FR}, maximum fluorescence in far-red; F_m’, maximum fluorescence in actinic red light; F_s^{FR}, steady state fluorescence in far red light; F_s, steady state fluorescence in actinic red light. Rates of net oxygen production (E) of photoautotrophically (PA WT) and photomixotrophically grown WT and ΔCytM were determined in cells taken on the third day of growth. O_2 production was initiated with white light (1000 μmol photons m^{-2} s^{-1}) in the absence (control) and in the presence of 0.5 mM DCBQ. Rates are expressed as μmol O_2 mg chl^{-1} h^{-1}, with DCBQ-treated WT considered as 100%. Values are means ± SD, n = four biological replicates. Asterisks indicate statistically significant differences (* P < 0.05, ** P <

0.001). Immunoblot analysis with D1-N antibody (F) was performed on samples taken on the third day. 15 µg total protein extract was loaded per 100% lane, 50% and 200% correspond to 7.5 µg and 30 µg, respectively.

Figure 4. Relaxation of flash-induced fluorescence yield in cells exposed to darkness. Subsequent relaxation of fluorescence yields in the dark was measured after a single-turnover saturating pulse in photomixotrophically cultured cells taken on the first (A), second (B), and third day (C) of cultivation. Growth conditions are described in Fig. 3. Prior to measurements, the cell suspension was adjusted to 5 µg chl ml^{-1}, resuspended in BG-11 supplemented with 10 mM glucose (C, D), and dark adapted for 5 min.

Figure 5. Redox kinetics of Cyt *f* in WT and ΔCytM cells. Cells were grown for three days under photoautotrophic (A) and photomixotrophic (B) conditions as described in Fig 3. Oxidation of Cyt *f* was induced by 500 µmol photons m^{-1} s^{-1} green light. When indicated, 20 µM DCMU was added prior the measurement. The curves were normalized to their respective maximal oxidation. The kinetics are representatives of three biological replicates.

Figure 6. Characterization of PSI in cells cultured photomixotrophically. The maximal amount of oxidizable P700, P_m (A), and immunoblotting of PSI reaction center protein, PsaB (B), was determined in cells cultured photomixotrophically. Values are means ± SD, n = three biological replicates. P700 oxidoreduction slow (C, D) and fast kinetics (E, F) were measured in parallel with fluorescence (Fig. 3). Fast kinetics curves (E, F) are normalized to P_m and referenced against their respective minimum P700 signal detected after the pulse. Cultivation, sample preparation, and experimental parameters are similar to those detailed in Fig. 3. P_0, initial P700; P_m^D, maximum P700 in darkness; P_m, maximum P700 under far-red light; P_m', maximum P700 under red actinic light.

Figure 7. O_2 and CO_2 fluxes in photomixotrophically cultured WT, ΔCytM, ΔCox/Cyd, and ΔCox/Cyd/CytM cells. Rates of O_2 and CO_2 fluxes in steady state (A). Values are means ± SD, n = 3-5 biological replicates. Total protein extracts were analysed by immunoblotting with *α*-Flv3-specific antibody (B). 15 µg total protein was loaded per 100% lane, 50% and 200% correspond to 7.5 µg and 30 µg, respectively. Kinetics of O_2 flux rates in whole cells (C-F). Cultivation, sample preparation, and experimental conditions are detailed in Fig. 3. In the light phase, 200 µmol photons m^{-2} s^{-1} constant white light was applied. Samples are supplemented by 1.5 mM $NaHCO_3$. Kinetics are representatives of 3-6 biological replicates. The source data of Fig. 7A can be found in Supplemental Table S2.

Figure 8. Characteristics at the sampling stage and functional classification of differentially regulated proteins in ΔCytM. Growth of the analysed cultures (A), with the ellipsis marking the sampling day. Cells were cultured similarly to those used in the biophysics analysis, except that the cells for proteomics were pre-cultivated under atmospheric CO_2 in order to fully adapt the cells to these conditions. Importantly, the extra pre-culturing step did not affect the growth of the experimental cultures. Values are means ± SD, n = 3 biological replicates. Relaxation of the flash-induced fluorescence yield in the dark

(B) was measured in the absence (closed symbols) and in the presence of 20 μM DCMU (open symbols). Differentially regulated proteins in ΔCytM were grouped according to their function (C). In total, 2415 proteins were identified, out of which 634 proteins were quantified and 162 were differentially regulated. The practical significance of differentially regulated proteins was set to fold change (FC) > 1.5 and FC < -1.5 ($P<0.05$). Effect of isoelectric point (pI) (D) and hydrophobicity (GRAVY) (E) of the proteins on the identification rate was determined. Black squares mark all of the 3507 predicted proteins in Synechocystis, lilac circles mark each protein identified in WT and in ΔCytM.

Fig. 9. Schematic showing changes in the metabolism in photomixotrophically grown ΔCytM cells compared to WT. Proteins, compounds, and metabolic routes with increased abundance or activity in ΔCytM relative to the WT are marked in green. Blue marks lower abundance in ΔCytM, grey marks unchanged, and white marks undetermined abundance or activity. TM, thylakoid membrane; PM, plasma membrane; C_i uptake, inorganic carbon uptake; C_o uptake, organic carbon uptake; EMP, Embden-Meyerhof-Parnas pathway; OPP, oxidative pentose phosphate pathway; ED, Entner-Doudoroff pathway; CB, Calvin-Benson cycle; TCA, tricarboxylic acid cycle; P_i uptake, inorganic phosphate uptake.

Figure 3. Fluorescence yield in WT and ΔCytM cells and quantification of O_2 production capacity during photomixotrophic growth. Chl fluorescence of photoautotrophically (A, B) and photomixotrophically (C, D) grown WT and ΔCytM whole cells. Photoautotrophic and photomixotrophic cultures were grown under constant 50 µmol photons m^{-2} s^{-1} illumination for three days, with or without 10 mM glucose, respectively. Prior to measurements, cells were resuspended in BG-11 supplemented with (C, D) and without (A,B) 10 mM glucose and dark adapted for 15 min. Maximum fluorescence was determined by applying a multiple turnover saturating pulse (500 ms, 5000 µmol photons m^{-2} s^{-1}) in darkness (black bars), under 40 W m^{-2} far-red light (brown bars) and under 50 µmol photons m^{-2} s^{-1} actinic red light (red bars). F_0, initial fluorescence; F_m^D, maximum fluorescence in dark; F_m^{FR}, maximum fluorescence in far-red; F_m', maximum fluorescence in actinic light; F_s^{FR}, steady state fluorescence in far red light. F_s, steady state fluorescence in actinic red light. Rates of net oxygen production (E) of photoautotrophically (PA WT) and photomixotrophically grown WT and ΔCytM were determined on the third day of growth. O_2 production was initiated with white light (1000 µmol photons m^{-2} s^{-1}) in the absence (control) and in the presence of 0.5 mM DCBQ. Values are means ± SD, n = four biological replicates. Asterisks indicate statistically significant differences (* $P < 0.05$, ** $P < 0.001$). Immunoblot analysis with D1-N antibody (F) was performed on samples taken on the third day. 15 µg total protein extract was loaded per 100% lane, 50% and 200% correspond to 7.5 µg and 30 µg, respectively.

Parsed Citations

Agarwal, R., Matros, A., Melzer, M., Mock, H.-P., Sainis, J.K., 2010. Heterogeneity in thylakoid membrane proteome of Synechocystis 6803. J. Proteomics 73, 976–991.
Pubmed: Author and Title
Google Scholar: Author Only Title Only Author and Title

Allahverdiyeva, Y., Isojärvi, J., Zhang, P., Aro, E.-M., 2015. Cyanobacterial Oxygenic Photosynthesis is Protected by Flavodiiron Proteins. Life (Basel, Switzerland) 5, 716–43.
Pubmed: Author and Title
Google Scholar: Author Only Title Only Author and Title

Allahverdiyeva, Y., Mustila, H., Ermakova, M., Bersanini, L., Richaud, P., Ajlani, G., Battchikova, N., Cournac, L., Aro, E.-M., 2013. Flavodiiron proteins Flv1 and Flv3 enable cyanobacterial growth and photosynthesis under fluctuating light. Proc. Natl. Acad. Sci. U. S. A. 110, 4111–6.
Pubmed: Author and Title
Google Scholar: Author Only Title Only Author and Title

Badger, M.R., Palmqvist, K., Yu, J.-W., 1994. Measurement of CO2 and HCO3- fluxes in cyanobacteria and microalgae during steady-state photosynthesis. Physiol. Plant. 90, 529–536.
Pubmed: Author and Title
Google Scholar: Author Only Title Only Author and Title

Baers, L.L., Breckels, L.M., Mills, L.A., Gatto, L., Deery, M., Stevens, T.J., Howe, C.J., Lilley, K.S., Lea-Smith, D.J., 2019. Proteome mapping of a cyanobacterium reveals distinct compartment organisation and cell-dispersed metabolism. Plant Physiol. pp.00897.2019.
Pubmed: Author and Title
Google Scholar: Author Only Title Only Author and Title

Beckmann, K., Messinger, J., Badger, M.R., Wydrzynski, T., Hillier, W., 2009. On-line mass spectrometry: membrane inlet sampling. Photosynth. Res. 102, 511–522.
Pubmed: Author and Title
Google Scholar: Author Only Title Only Author and Title

Bernroitner, M., Tangl, D., Lucini, C., Furtmüller, P.G., Peschek, G.A., Obinger, C., 2009. Cyanobacterial cytochrome cM: Probing its role as electron donor for CuA of cytochrome c oxidase. Biochim. Biophys. Acta - Bioenerg. 1787, 135–143.
Pubmed: Author and Title
Google Scholar: Author Only Title Only Author and Title

Bialek, W., Nelson, M., Tamiola, K., Kallas, T., Szczepaniak, A., 2008. Deeply branching c6-like cytochromes of cyanobacteria. Biochemistry 47, 5515–5522.
Pubmed: Author and Title
Google Scholar: Author Only Title Only Author and Title

Bialek, W., Szczepaniak, A., Kolesinski, P., Kallas, T., 2016. Cryptic c 6-Like and c M Cytochromes of Cyanobacteria. In: Cytochrome Complexes: Evolution, Structures, Energy Transduction, and Signaling. Dordrecht: Springer, pp. 713–734.
Pubmed: Author and Title
Google Scholar: Author Only Title Only Author and Title

Bothe, H., Schmitz, O., Yates, M.G., Newton, W.E., 2010. Nitrogen fixation and hydrogen metabolism in cyanobacteria. Microbiol. Mol. Biol. Rev. 74, 529–51.
Pubmed: Author and Title
Google Scholar: Author Only Title Only Author and Title

Brown, K.A., Guo, Z., Tokmina-Lukaszewska, M., Scott, L.W., Lubner, C.E., Smolinski, S., Mulder, D.W., Bothner, B., King, P.W., 2019. The oxygen reduction reaction catalyzed by Synechocystis sp. PCC 6803 flavodiiron proteins. Sustain. Energy Fuels 3, 3191–3200.
Pubmed: Author and Title
Google Scholar: Author Only Title Only Author and Title

Büsch, A., Friedrich, B., Cramm, R., 2002. Characterization of the norB gene, encoding nitric oxide reductase, in the nondenitrifying cyanobacterium Synechocystis sp. strain PCC6803. Appl. Environ. Microbiol. 68, 668–72.
Pubmed: Author and Title
Google Scholar: Author Only Title Only Author and Title

Casella, S., Huang, F., Mason, D., Zhao, G.-Y., Johnson, G.N., Mullineaux, C.W., Liu, L.-N., 2017. Dissecting the Native Architecture and Dynamics of Cyanobacterial Photosynthetic Machinery. Mol. Plant 10, 1434–1448.
Pubmed: Author and Title
Google Scholar: Author Only Title Only Author and Title

Chandramouli, K., Qian, P.-Y., 2009. Proteomics: challenges, techniques and possibilities to overcome biological sample complexity. Hum. Genomics Proteomics 2009.
Pubmed: Author and Title
Google Scholar: Author Only Title Only Author and Title

Cho, Y.S., Pakrasi, H.B., Whitmarsh, J., 2000. Cytochrome cM from Synechocystis 6803. Eur. J. Biochem. 267, 1068–1074.

Pubmed: Author and Title
Google Scholar: Author Only Title Only Author and Title

Deák, Z., Sass, L., Kiss, É., Vass, I., 2014. Characterization of wave phenomena in the relaxation of flash-induced chlorophyll fluorescence yield in cyanobacteria. Biochim. Biophys. Acta - Bioenerg. 1837, 1522–1532.
Pubmed: Author and Title
Google Scholar: Author Only Title Only Author and Title

Durán, R. V, Hervás, M., De La Rosa, M.A., Navarro, J.A., 2004. The efficient functioning of photosynthesis and respiration in Synechocystis sp. PCC 6803 strictly requires the presence of either cytochrome c6 or plastocyanin. J. Biol. Chem. 279, 7229–33.
Pubmed: Author and Title
Google Scholar: Author Only Title Only Author and Title

Ermakova, M., Huokko, T., Richaud, P., Bersanini, L., Howe, C.J., Lea-Smith, D.J., Peltier, G., Allahverdiyeva, Y., 2016. Distinguishing the Roles of Thylakoid Respiratory Terminal Oxidases in the Cyanobacterium Synechocystis sp. PCC 6803. Plant Physiol. 171, 1307–19.
Pubmed: Author and Title
Google Scholar: Author Only Title Only Author and Title

Haimovich-Dayan, M., Kahlon, S., Hihara, Y., Hagemann, M., Ogawa, T., Ohad, I., Lieman-Hurwitz, J., Kaplan, A., 2011. Cross-talk between photomixotrophic growth and CO2-concentrating mechanism in Synechocystis sp. strain PCC 6803. Environ. Microbiol. 13, 1767–1777.
Pubmed: Author and Title
Google Scholar: Author Only Title Only Author and Title

Heinz, S., Liauw, P., Nickelsen, J., Nowaczyk, M., 2016. Analysis of photosystem II biogenesis in cyanobacteria. Biochim. Biophys. Acta - Bioenerg. 1857, 274–287.
Pubmed: Author and Title
Google Scholar: Author Only Title Only Author and Title

Helman, Y., Tchernov, D., Reinhold, L., Shibata, M., Ogawa, T., Schwarz, R., Ohad, I., Kaplan, A., 2003. Genes encoding A-type flavoproteins are essential for photoreduction of O2 in cyanobacteria. Curr. Biol. 13, 230–5.
Pubmed: Author and Title
Google Scholar: Author Only Title Only Author and Title

Hieronymi, M., Macke, A., 2010. Spatiotemporal underwater light field fluctuations in the open ocean. J. Eur. Opt. Soc. Rapid Publ. 5, 10019s.
Pubmed: Author and Title
Google Scholar: Author Only Title Only Author and Title

Hiraide, Y., Oshima, K., Fujisawa, T., Uesaka, K., Hirose, Y., Tsujimoto, R., Yamamoto, H., Okamoto, S., Nakamura, Y., Terauchi, K., Omata, T., Ihara, K., Hattori, M., Fujita, Y., 2015. Loss of cytochrome cM stimulates cyanobacterial heterotrophic growth in the dark. Plant Cell Physiol. 56, 334–45.
Pubmed: Author and Title
Google Scholar: Author Only Title Only Author and Title

Hoch, G., Kok, B., 1963. A mass spectrometer inlet system for sampling gases dissolved in liquid phases. Arch. Biochem. Biophys. 101, 160–170.
Pubmed: Author and Title
Google Scholar: Author Only Title Only Author and Title

Huokko, T., Muth-Pawlak, D., Aro, E.-M., 2019. Thylakoid Localized Type 2 NAD(P)H Dehydrogenase NdbA Optimizes Light-Activated Heterotrophic Growth of Synechocystis sp. PCC 6803. Plant Cell Physiol. 60, 1386–1399.
Pubmed: Author and Title
Google Scholar: Author Only Title Only Author and Title

Huokko, T., Muth-Pawlak, D., Battchikova, N., Allahverdiyeva, Y., Aro, E., 2017. Role of Type 2 NAD(P)H Dehydrogenase NdbC in Redox Regulation of Carbon Allocation in Synechocystis. Plant Physiol. 174, 1863–1880.
Pubmed: Author and Title
Google Scholar: Author Only Title Only Author and Title

Ittekkot, V., Brockmann, U., Michaelis, W., Degens, E., 1981. Dissolved Free and Combined Carbohydrates During a Phytoplankton Bloom in the Northern North Sea. Mar. Ecol. Prog. Ser. 4, 299–305.
Pubmed: Author and Title
Google Scholar: Author Only Title Only Author and Title

Kaňa, R., 2013. Mobility of photosynthetic proteins. Photosynth. Res. 116, 465–479.
Pubmed: Author and Title
Google Scholar: Author Only Title Only Author and Title

Kerfeld, C.A., Krogmann, D.W., 1998. Photosynthetic cytochromes c in cyanobacteria, algae and plants. Annu. Rev. Plant Physiol. Plant Mol. Biol. 49, 397–425.
Pubmed: Author and Title
Google Scholar: Author Only Title Only Author and Title

Klughammer, C., Schreiber, U., 2008a. Complementary PS II quantum yields calculated from simple fluorescence parameters measured

by PAM fluorometry and the Saturation Pulse method. PAM Appl. Notes 1, 27–35.
Pubmed: Author and Title
Google Scholar: Author Only Title Only Author and Title

Klughammer, C., Schreiber, U., 2008b. Saturation Pulse method for assessment of energy conversion in PS I. PAM Appl. Notes 1, 11–14.
Pubmed: Author and Title
Google Scholar: Author Only Title Only Author and Title

Kranzler, C., Lis, H., Finkel, O.M., Schmetterer, G., Shaked, Y., Keren, N., 2014. Coordinated transporter activity shapes high-affinity iron acquisition in cyanobacteria. ISME J. 8, 409–17.
Pubmed: Author and Title
Google Scholar: Author Only Title Only Author and Title

Lea-Smith, David J., Bombelli, P., Vasudevan, R., Howe, C.J., 2016. Photosynthetic, respiratory and extracellular electron transport pathways in cyanobacteria. Biochim. Biophys. Acta - Bioenerg. 1857, 247–255.
Pubmed: Author and Title
Google Scholar: Author Only Title Only Author and Title

Lea-Smith, D.J., Ross, N., Zori, M., Bendall, D.S., Dennis, J.S., Scott, S. a, Smith, A.G., Howe, C.J., 2013. Thylakoid terminal oxidases are essential for the cyanobacterium Synechocystis sp. PCC 6803 to survive rapidly changing light intensities. Plant Physiol. 162, 484–95.
Pubmed: Author and Title
Google Scholar: Author Only Title Only Author and Title

Lea-Smith, David J, Vasudevan, R., Howe, C.J., 2016. Generation of Marked and Markerless Mutants in Model Cyanobacterial Species. J. Vis. Exp.
Pubmed: Author and Title
Google Scholar: Author Only Title Only Author and Title

Lee, S., Ryu, J.-Y., Kim, S.Y., Jeon, J.-H., Song, J.Y., Cho, H.-T., Choi, S.-B., Choi, D., de Marsac, N.T., Park, Y.-I., 2007. Transcriptional regulation of the respiratory genes in the cyanobacterium Synechocystis sp. PCC 6803 during the early response to glucose feeding. Plant Physiol. 145, 1018–30.
Pubmed: Author and Title
Google Scholar: Author Only Title Only Author and Title

Liu, L.-N., Bryan, S.J., Huang, F., Yu, J., Nixon, P.J., Rich, P.R., Mullineaux, C.W., 2012. Control of electron transport routes through redox-regulated redistribution of respiratory complexes. Proc. Natl. Acad. Sci. 109, 11431–11436.
Pubmed: Author and Title
Google Scholar: Author Only Title Only Author and Title

Malakhov, M.P., Malakhova, O.A., Murata, N., 1999. Balanced regulation of expression of the gene for cytochrome cM and that of genes for plastocyanin and cytochrome c6 in Synechocystis. FEBS Lett. 444, 281–284.
Pubmed: Author and Title
Google Scholar: Author Only Title Only Author and Title

Malakhov, M.P., Wada, H., Los, D.A., Semenenko, V.E., Murata, N., 1994. A New Type of Cytochrome c from Synechocystis PCC6803. J. Plant Physiol. 144, 259–264.
Pubmed: Author and Title
Google Scholar: Author Only Title Only Author and Title

Manna, P., Vermaas, W., 1997. Lumenal proteins involved in respiratory electron transport in the cyanobacterium Synechocystis sp. PCC6803. Plant Mol. Biol. 35, 407–416.
Pubmed: Author and Title
Google Scholar: Author Only Title Only Author and Title

Molina-Heredia, F.P., Balme, A., Hervás, M., Navarro, J.A., De la Rosa, M.A., 2002. A comparative structural and functional analysis of cytochrome c M , cytochrome c 6 and plastocyanin from the cyanobacterium Synechocystis sp. PCC 6803. FEBS Lett. 517, 50–54.
Pubmed: Author and Title
Google Scholar: Author Only Title Only Author and Title

Moore, L.R., 2013. More mixotrophy in the marine microbial mix. Proc. Natl. Acad. Sci. 110, 8323–8324.
Pubmed: Author and Title
Google Scholar: Author Only Title Only Author and Title

Mullineaux, C.W., 2014. Co-existence of photosynthetic and respiratory activities in cyanobacterial thylakoid membranes. Biochim. Biophys. Acta - Bioenerg. 1837, 503–511.
Pubmed: Author and Title
Google Scholar: Author Only Title Only Author and Title

Mustila, H., Paananen, P., Battchikova, N., Santana-Sánchez, A., Muth-Pawlak, D., Hagemann, M., Aro, E.-M., Allahverdiyeva, Y., 2016. The Flavodiiron Protein Flv3 Functions as a Homo-Oligomer During Stress Acclimation and is Distinct from the Flv1/Flv3 Hetero-Oligomer Specific to the O2 Photoreduction Pathway. Plant Cell Physiol.
Pubmed: Author and Title
Google Scholar: Author Only Title Only Author and Title

Ogawa, T., 1991. A gene homologous to the subunit-2 gene of NADH dehydrogenase is essential to inorganic carbon transport of Synechocystis PCC6803. Proc. Natl. Acad. Sci. 88, 4275–4279.
Pubmed: Author and Title
Google Scholar: Author Only Title Only Author and Title

Perez-Riverol, Y., Csordas, A., Bai, J., Bernal-Llinares, M., Hewapathirana, S., Kundu, D.J., Inuganti, A., Griss, J., Mayer, G., Eisenacher, M., Pérez, E., Uszkoreit, J., Pfeuffer, J., Sachsenberg, T., Yilmaz, S., Tiwary, S., Cox, J., Audain, E., Walzer, M., Jarnuczak, A.F., Ternent, T., Brazma, A., Vizcaíno, J.A., 2019. The PRIDE database and related tools and resources in 2019: improving support for quantification data. Nucleic Acids Res. 47, D442–D450.
Pubmed: Author and Title
Google Scholar: Author Only Title Only Author and Title

Pils, D., 1997. Evidence for in vivo activity of three distinct respiratory terminal oxidases in the cyanobacterium Synechocystis sp. strain PCC6803. FEMS Microbiol. Lett. 152, 83–88.
Pubmed: Author and Title
Google Scholar: Author Only Title Only Author and Title

Ried, J.L., Collmer, A., 1987. An nptI-sacB-sacR cartridge for constructing directed, unmarked mutations in gram-negative bacteria by marker exchange-eviction mutagenesis. Gene 57, 239–46.
Pubmed: Author and Title
Google Scholar: Author Only Title Only Author and Title

Santana-Sanchez, A., Solymosi, D., Mustila, H., Bersanini, L., Aro, E.-M., Allahverdiyeva, Y., 2019. Flavodiiron proteins 1–to-4 function in versatile combinations in O2 photoreduction in cyanobacteria. Elife 8.
Pubmed: Author and Title
Google Scholar: Author Only Title Only Author and Title

Schorsch, M., Kramer, M., Goss, T., Eisenhut, M., Robinson, N., Osman, D., Wilde, A., Sadaf, S., Brückler, H., Walder, L., Scheibe, R., Hase, T., Hanke, G.T., 2018. A unique ferredoxin acts as a player in the low-iron response of photosynthetic organisms. Proc. Natl. Acad. Sci. U. S. A. 115, E12111–E12120.
Pubmed: Author and Title
Google Scholar: Author Only Title Only Author and Title

Schottkowski, M., Ratke, J., Oster, U., Nowaczyk, M., Nickelsen, J., 2009. Pitt, a Novel Tetratricopeptide Repeat Protein Involved in Light-Dependent Chlorophyll Biosynthesis and Thylakoid Membrane Biogenesis in Synechocystis sp. PCC 6803. Mol. Plant 2, 1289–1297.
Pubmed: Author and Title
Google Scholar: Author Only Title Only Author and Title

Schuller, J.M., Birrell, J.A., Tanaka, H., Konuma, T., Wulfhorst, H., Cox, N., Schuller, S.K., Thiemann, J., Lubitz, W., Sétif, P., Ikegami, T., Engel, B.D., Kurisu, G., Nowaczyk, M.M., 2019. Structural adaptations of photosynthetic complex I enable ferredoxin-dependent electron transfer. Science (80-.). 363, 257–260.
Pubmed: Author and Title
Google Scholar: Author Only Title Only Author and Title

Schultze, M., Forberich, B., Rexroth, S., Dyczmons, N.G., Roegner, M., Appel, J., 2009. Localization of cytochrome b6f complexes implies an incomplete respiratory chain in cytoplasmic membranes of the cyanobacterium Synechocystis sp. PCC 6803. Biochim. Biophys. Acta - Bioenerg. 1787, 1479–1485.
Pubmed: Author and Title
Google Scholar: Author Only Title Only Author and Title

Shen, J.R., Inoue, Y., 1993. Binding and functional properties of two new extrinsic components, cytochrome c-550 and a 12-kDa protein, in cyanobacterial photosystem II. Biochemistry 32, 1825–1832.
Pubmed: Author and Title
Google Scholar: Author Only Title Only Author and Title

Shpilyov, A. V., Zinchenko, V. V., Shestakov, S. V., Grimm, B., Lokstein, H., 2005. Inactivation of the geranylgeranyl reductase (ChlP) gene in the cyanobacterium Synechocystis sp. PCC 6803. Biochim. Biophys. Acta - Bioenerg. 1706, 195–203.
Pubmed: Author and Title
Google Scholar: Author Only Title Only Author and Title

Smith, A.J., 1983. Modes of cyanobacterial carbon metabolism. Ann. l'Institut Pasteur / Microbiol. 134, 93–113.
Pubmed: Author and Title
Google Scholar: Author Only Title Only Author and Title

Sonoda, M., Kitano, K., Katoh, A., Katoh, H., Ohkawa, H., Ogawa, T., 1997. Size of cotA and identification of the gene product in Synechocystis sp. strain PCC6803. J. Bacteriol. 179, 3845–3850.
Pubmed: Author and Title
Google Scholar: Author Only Title Only Author and Title

Srivastava, A., Strasser, R.J., Govindjee, 1995. Differential effects of dimethylbenzoquinone and dichlorobenzoquinone on chlorophyll fluorescence transient in spinach thylakoids. J. Photochem. Photobiol. B Biol. 31, 163–169.
Pubmed: Author and Title
Google Scholar: Author Only Title Only Author and Title

Stal, L.J., Moezelaar, R., 1997. Fermentation in cyanobacteria. FEMS Microbiol. Rev. 21, 179–211.
Pubmed: Author and Title
Google Scholar: Author Only Title Only Author and Title

Sültemeyer, D., Price, G.D., Yu, J.-W., Badger, M.R., 1995. Characterisation of carbon dioxide and bicarbonate transport during steady-state photosynthesis in the marine cyanobacterium Synechococcus strain PCC7002. Planta.
Pubmed: Author and Title
Google Scholar: Author Only Title Only Author and Title

Sun, N., Han, X., Xu, M., Kaplan, A., Espie, G.S., Mi, H., 2018. A thylakoid-located carbonic anhydrase regulates CO 2 uptake in the cyanobacterium Synechocystis sp. PCC 6803. New Phytol. nph.15575.
Pubmed: Author and Title
Google Scholar: Author Only Title Only Author and Title

Takahashi, H., Uchimiya, H., Hihara, Y., 2008. Difference in metabolite levels between photoautotrophic and photomixotrophic cultures of Synechocystis sp. PCC 6803 examined by capillary electrophoresis electrospray ionization mass spectrometry. J. Exp. Bot. 59, 3009–18.
Pubmed: Author and Title
Google Scholar: Author Only Title Only Author and Title

Teeling, H., Fuchs, B.M., Becher, D., Klockow, C., Gardebrecht, A., Bennke, C.M., Kassabgy, M., Huang, S., Mann, A.J., Waldmann, J., Weber, M., Klindworth, A., Otto, A., Lange, J., Bernhardt, J., Reinsch, C., Hecker, M., Peplies, J., Bockelmann, F.D., Callies, U., Gerdts, G., Wichels, A., Wiltshire, K.H., Glöckner, F.O., Schweder, T., Amann, R., 2012. Substrate-controlled succession of marine bacterioplankton populations induced by a phytoplankton bloom. Science 336, 608–611.
Pubmed: Author and Title
Google Scholar: Author Only Title Only Author and Title

Vermaas, W.F.J., 2001. Photosynthesis and respiration in cyanobacteria. In: Encyclopedia of Life Sciences. pp. 1–7.
Pubmed: Author and Title
Google Scholar: Author Only Title Only Author and Title

Vicente, J.B., Gomes, C.M., Wasserfallen, A., Teixeira, M., 2002. Module fusion in an A-type flavoprotein from the cyanobacterium Synechocystis condenses a multiple-component pathway in a single polypeptide chain. Biochem. Biophys. Res. Commun. 294, 82–87.
Pubmed: Author and Title
Google Scholar: Author Only Title Only Author and Title

Wegener, K.M., Welsh, E.A., Thornton, L.E., Keren, N., Jacobs, J.M., Hixson, K.K., Monroe, M.E., Camp, D.G., Smith, R.D., Pakrasi, H.B., 2008. High sensitivity proteomics assisted discovery of a novel operon involved in the assembly of photosystem II, a membrane protein complex. J. Biol. Chem. 283, 27829–37.
Pubmed: Author and Title
Google Scholar: Author Only Title Only Author and Title

Willows, R.D., Mayer, S.M., Foulk, M.S., DeLong, A., Hanson, K., Chory, J., Beale, S.I., 2000. Phytobilin biosynthesis: the Synechocystis sp. PCC 6803 heme oxygenase-encoding ho1 gene complements a phytochrome-deficient Arabidopsis thaliana hy1 mutant. Plant Mol. Biol. 43, 113–120.
Pubmed: Author and Title
Google Scholar: Author Only Title Only Author and Title

Wu, Q., Vermaas, W.F., 1995. Light-dependent chlorophyll a biosynthesis upon chlL deletion in wild-type and photosystem I-less strains of the cyanobacterium Synechocystis sp. PCC 6803. Plant Mol. Biol. 29, 933–45.
Pubmed: Author and Title
Google Scholar: Author Only Title Only Author and Title

Zilliges, Y., Dau, H., 2016. Unexpected capacity for organic carbon assimilation by Thermosynechococcus elongatus, a crucial photosynthetic model organism. FEBS Lett. 590, 962–970.
Pubmed: Author and Title
Google Scholar: Author Only Title Only Author and Title

Zubkov, M. V., Tarran, G.A., 2008. High bacterivory by the smallest phytoplankton in the North Atlantic Ocean. Nature 455, 224–226.
Pubmed: Author and Title
Google Scholar: Author Only Title Only Author and Title